GCA-TR-69-8-N

STUDIES IN PLANETARY METEOROLOGY

By George Ohring

GCA CORPORATION
GCA TECHNOLOGY DIVISION
Bedford, Massachusetts

ANNUAL TECHNICAL REPORT

Contract No. NASW-1725

April 1969

Prepared for

NATIONAL AERONAUTICS AND SPACE ADMINISTRATION
Headquarters
Washington, D. C.

TABLE OF CONTENTS

TABLE OF CONTENTS (continued)

STUDIES IN PLANETARY METEOROLOGY

By George Ohring
GCA CORPORATION
GCA TECHNOLOGY DIVISION
Bedford, Massachusetts

SUMMARY

This annual technical report consists of three papers which report the results of studies conducted during the past year on the meteorology of the atmosphere of Venus. These studies include an evaluation of the greenhouse explanation of the high Venusian surface temperature, computations of the radiative equilibrium temperature distribution in the Venusian atmosphere, and empirical fits of infrared transmittance tables for application to Venus. Complete abstracts of these studies may be found with the respective papers.

PART 1

HIGH SURFACE TEMPERATURE ON VENUS: EVALUATION OF THE GREENHOUSE EXPLANATION

George Ohring

HIGH SURFACE TEMPERATURE ON VENUS: EVALUATION OF THE GREENHOUSE EXPLANATION

ABSTRACT

Calculations of the mean surface temperature of Venus are performed with a simple non-grey radiation balance model. The model is based upon a balance of net incoming solar radiation and emerging thermal radiation at the top of the atmosphere. To calculate the emerging thermal radiation, it is assumed that the shape of the vertical temperature profile is similar to that observed by Mariner 5 and Venera 4 - that is, a constant lapse-rate of 9°C/km from the surface to a pressure level of a few tenths of an atmosphere, above which the temperature remains constant. Given the atmospheric composition, cloud transmittance in the infrared, and surface pressure, the surface temperature can be determined from the balance requirement at the top of the atmosphere. Calculations are performed for a low surface pressure (20 atm) and high surface pressure (65 atm) model. For a pure carbon dioxide atmosphere, the results indicate that mean surface temperatures of 500°K to 600°K can be maintained in the 20 atm model, and 650°K to 700°K in the 65 atm model, if water vapor mixing ratios are of the order of 10^{-3}. In the event the water vapor constant is lower, similar surface temperatures can be maintained if the clouds are moderately opaque in the infrared (transmittance of ~ 0.1).

INTRODUCTION

The high surface temperature of Venus ($\sim 600^{\circ}K$ to $700^{\circ}K$) inferred from microwave observations has now been confirmed by the direct in-situ observations performed by the Soviet spacecraft Venera 4 (ref. 1). A major problem of planetary meteorology is to understand why Venus is so hot.

In the absence of an atmosphere, the mean radiative equilibrium temperature of a planet depends only upon its distance from the sun and its albedo. This temperature can be computed from an equation representing a balance between the planet's blackbody emission of thermal radiation and its absorption of solar radiation.

$$\sigma T_e^4 = \frac{S.C.}{4 R^2} (1 - A) \qquad (1)$$

where σ is the Stefan-Boltzmann constant, S.C. is the solar constant (intensity of solar radiation at Earth's distance from the sun), R is the planet's distance from the sun in astronomical units (Earth-sun distance = 1), and A is the planet's albedo. Figure 1 shows the radiative equilibrium temperatures of Mars, Venus, and Earth for a range of possible albedos for these planets. This figure shows that Venus and Earth would have similar mean radiative equilibrium temperatures in the absence of atmospheres. The presence of an atmosphere introduces a greenhouse effect which raises the surface temperature. For Mars and Earth, this effect is rather modest. The greenhouse effect on Earth causes an increase of about $35^{\circ}K$, resulting in an average surface temperature of $288^{\circ}K$. On Mars, the increase is about $7^{\circ}K$, resulting in an average surface temperature of about $215^{\circ}K$. Arguing by analogy, one would expect the mean surface temperature of Venus also to be not much higher than the radiative equilibrium value computed in the absence of an atmosphere. Thus, a mean temperature of about $300^{\circ}K$ might be expected for Venus. The observed surface temperature is about twice this value. The problem is to explain the cause of the high observed surface temperature.

An extreme greenhouse effect as an explanation for the high surface temperature was suggested by Sagan (ref. 2). Since this suggestion was made, various investigators have attempted to evaluate the greenhouse effect on Venus (ref. 3 - 6). Most of the greenhouse research has centered around the question of whether there are sufficient amounts of infrared absorbing gases in the atmosphere to maintain the high surface temperatures. However, Ohring and Mariano (ref. 5) included the effect of an infrared absorbing cloud layer, while Samuelson (ref. 6) neglected gaseous absorption and computed the greenhouse effect for a semi-

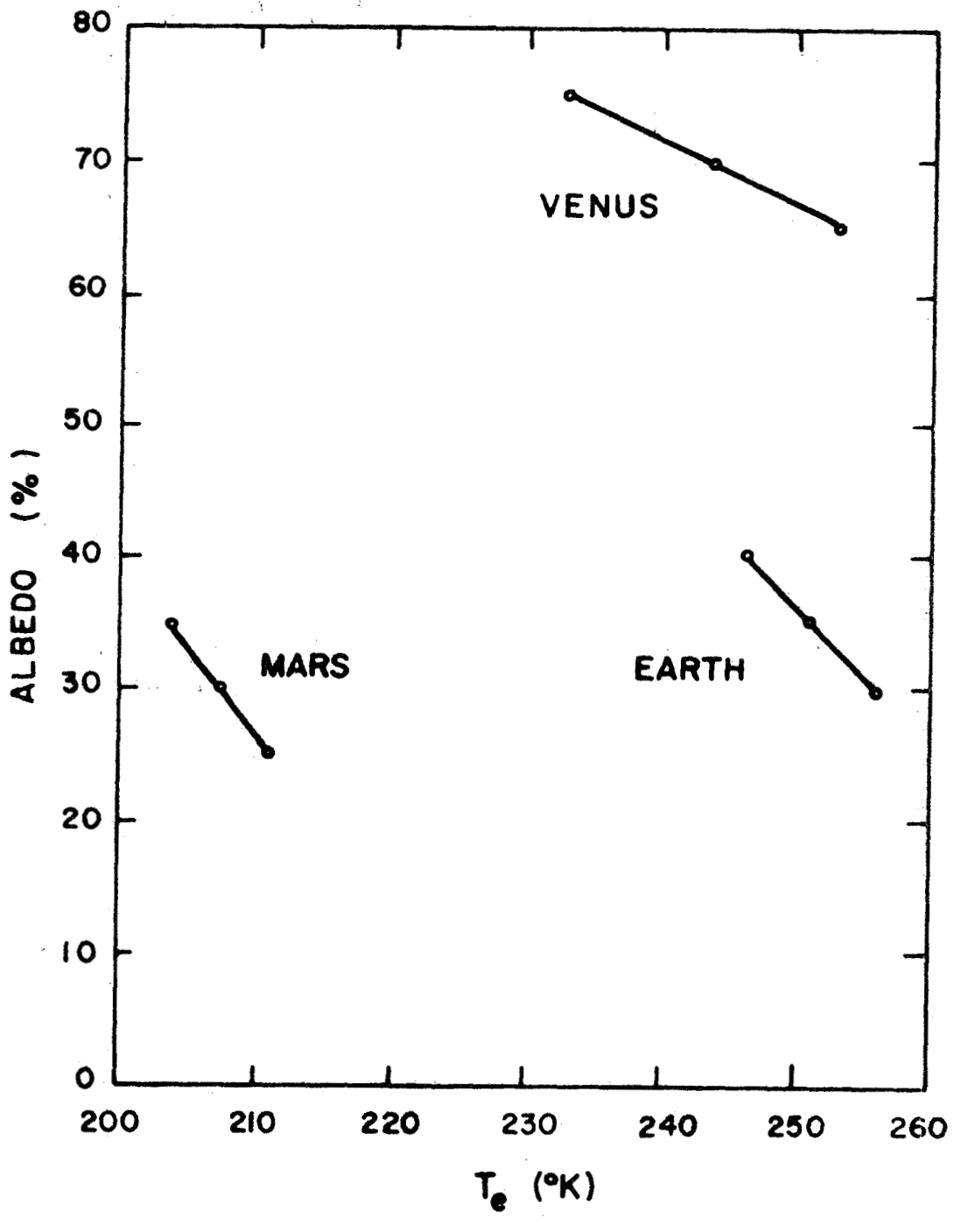

Figure 1. Radiative equilibrium temperatures of Earth, Mars and Venus.

infinite particulate layer. These evaluations have been rather crude, since grey radiative models have been used and since important parameters, such as atmospheric composition and surface pressure, were really unknown. The results have also conflicted. Based upon the results to date, the greenhouse explanation of the high surface temperature is still in doubt.

In the present study, we use the recent Mariner 5 and Venera 4 observations of temperature, pressure and atmospheric composition to evaluate the greenhouse effect on Venus with the use of a non-grey radiative model.

APPROACH AND PROCEDURES

Our approach is based upon the condition of radiation balance that must prevail at the top of the Venusian atmosphere if the planet's mean temperature is in a steady state condition. This balance is between the net incoming solar radiation and the thermal radiation emerging from the planet-atmosphere system. The net incoming solar radiation is known, being a function only of the solar constant, the planet's distance from the sun, and its albedo. The emerging thermal radiation depends upon the surface temperature and vertical temperature profile in the atmosphere, and the atmospheric composition and pressure. If we assume that the form of the vertical temperature structure, and the atmospheric composition and surface pressure are known, we can determine the surface temperature that yields the required balance at the top of the atmosphere. The computed surface temperature can then be compared to the observed surface temperature. The information on form of the temperature profile and atmospheric composition and surface pressure will be based mainly upon the Venera 4 and Mariner 5 observations.

The radiative flux emerging from a planetary atmosphere in a spectral interval r can be written as

$$F_r = \int_{\tau_r(s)}^{1} B_r(T)\,d\tau_r + B_r(T_s)\,\tau_r(s) \qquad (2)$$

where τ_r is the flux transmittance of atmospheric gases for the spectral interval, B_r is the blackbody flux in the spectral interval, T is temperature, and s refers to surface values. In this equation, the transmittance, τ, represents the vertical coordinate; it decreases from unity at the top of the atmosphere to the value $\tau(s)$ at the surface. To obtain the total outgoing radiative energy flux, one must integrate over all spectral intervals r. Thus,

$$F = \sum_{i=1}^{m} F_r \qquad (3)$$

where m is the number of spectral intervals. The total radiative energy flux emerging from the atmosphere must, in the mean, balance the net incoming solar radiation. Thus,

$$F = \sigma T_e^4 \qquad (4)$$

where T_e is the effective temperature of the net incoming solar radiation as derived from Equation (1).

radiation as derived from Equation (1).

Equation (2) does not include the effect of a cloud layer on the emerging radiative flux. Since very little is known about the Venusian cloud layer, we shall incorporate its effect on the emerging radiative flux in as simple a manner as possible. We shall assume that the cloud is located at a pressure level P_{cld} and that it has a grey infrared transmittance τ_{cld}. In the presence of such a cloud, the contribution of the atmosphere below the cloud to the emerging radiative flux at the top of the atmosphere is reduced by the factor τ_{cld}. Equation (2) then becomes

$$F_r = \int_{\tau_{cld}\cdot\tau_r(P_{cld})}^{1} B_r(T)\, d\tau_r + \tau_{cld}\left[\int_{\tau_r(s)}^{\tau_r(P_{cld})} B_r(T) d\tau_r + B_r(T_s)\tau_r(s)\right] \quad (5)$$

The vertical temperature profile derived from the Mariner 5 and Venera 4 observations is characterized by a lower atmospheric layer with an approximately linear lapse-rate of $9^{\circ}K/km$ and an upper layer that is approximately isothermal. Thus, given the height of the tropopause - the level separating the two layers - the entire vertical temperature profile becomes a function only of the surface temperature. The surface temperature that balances Equation (4) can be computed by an iterative technique. The concept is illustrated schematically in Figure 2. The temperature profile associated with the surface temperature $T_s(1)$ yields an emerging radiative flux less than the net incoming solar radiation. The temperature profile associated with $T_s(2)$ yields an emerging flux greater than the net incoming solar radiation. Between these two temperature profiles is one that yields an emerging flux which exactly balances the net incoming solar radiation. The iteration procedure used to arrive at the final surface temperature consists of the following steps.

(1) With a first guess of the surface temperature, T(n), the emerging radiation, F(n), is calculated.

(2) A new surface temperature is obtained from

$$T(n+1) = \left(\frac{\sigma T_e^4}{F(n)}\right)^{1/4} T(n). \quad (6)$$

This iteration equation assumes that the emerging fluxes are proportional to the fourth power of the surface temperature.

(3) The emerging radiation is recalculated with the new temperature structure.

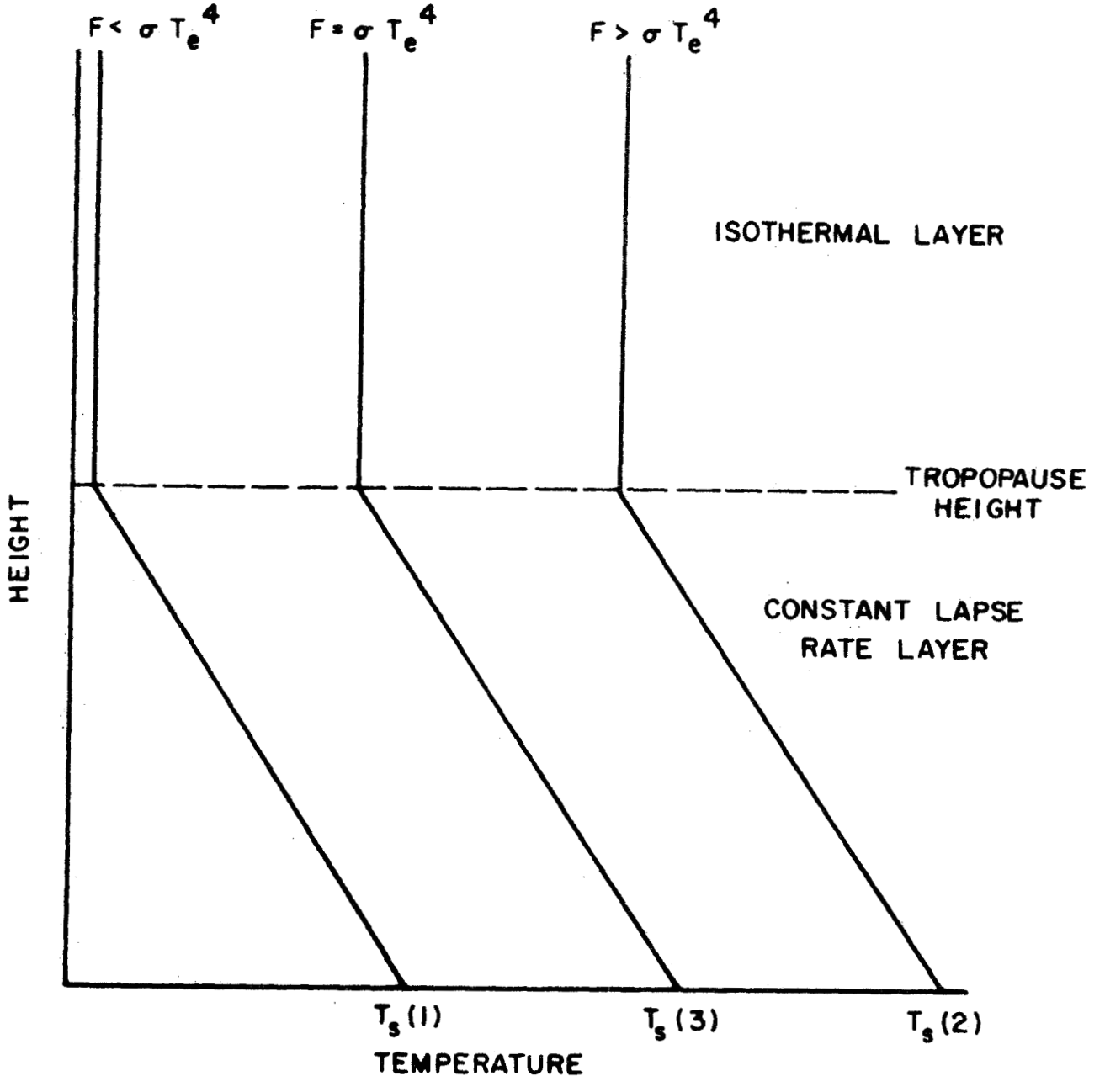

Figure 2. Schematic illustration of assumed vertical temperature structure and technique for deriving surface temperature that leads to balance between emerging and net incoming radiation.

(4) This procedure continues until the difference in successive surface temperatures is less than one degree Kelvin, indicating a balance between emerging and net incoming radiation. In practice, only a few iterations are required to arrive at a final surface temperature.

Gases contributing to the greenhouse effect of the Venus atmosphere are carbon dioxide and water vapor. Experimental transmittance data for CO_2 and H_2O for the high pressures and path lengths applicable to the Venus atmosphere are not available. Available laboratory data for CO_2, for example, cover a range of pressures up to a few atmospheres and CO_2 amounts up to about 10^4 atmo-cm (see, for example, ref. 7). The surface temperature on Venus is tens of atmospheres and the amount of CO_2 is of the order of 10^7 atmo-cm. The available laboratory data and theoretical calculations have been fit to a theoretical strong line absorption law by Bartko and Hanel (ref. 8), who utilized the resulting transmittance formulas for calculations of radiative equilibrium temperature distributions above the clouds of Venus. These strong line fits should also be applicable at the elevated pressures and long path lengths of the lower Venusian atmosphere, and we adopt them in the present study.

The transmittance of a spectral interval r is expressed as

$$\tau_r = \exp\left[-(m_r u_r^*)^{n_r}\right] \tag{7}$$

where m_r and n_r are constants for the spectral interval, and u_r^*, the effective absorber amount, is given by

$$u_r^* = 1.66\, u\left(\frac{T_o}{\bar{T}}\right)^{3/2} \exp\left[\gamma_r\left(\frac{1}{T_o} - \frac{1}{\bar{T}}\right)\right]\left(\frac{\bar{p}}{p_o}\right)^{k_r} \tag{8}$$

where u is the path length of the absorbing gas in units of atmo-cm for CO_2 and g cm^{-2} for H_2O, T_o and p_o are standard temperature and pressure, respectively, $\bar{T}$ and $\bar{p}$ are the average temperature and pressure along the path, γ_r is a temperature coefficient, and $k_r = 2n_r$. The factor 1.66 is introduced to approximate flux transmission. The CO_2 path length between a pressure level p and the top of the atmosphere is given by

$$u_{CO_2} = \frac{cp}{g\,\rho'_{CO_2}} \tag{9}$$

where c is the CO_2 mass concentration, g is the Venusian acceleration

of gravity, ρ_{CO_2} is the density of CO_2 at STP. The H_2O path length between pressure level p and the top of the atmosphere is

$$u_{H_2O} = \frac{wp}{g} \tag{10}$$

where w is the H_2O mixing ratio.

The constants for all the spectral intervals, (after ref. 8), are tabulated in Table 1. In those intervals in which both CO_2 and H_2O absorb, the total transmittance is given by the product of the individual transmittances.

To evaluate Equation (2), expressions for B_r, the blackbody flux in a spectral interval, are required. The blackbody flux in any spectral interval r bounded by wavenumbers ν_1 and ν_2 may be written as

$$B_r = \pi \int_{\nu_1}^{\nu_2} B_\nu \, d\nu = \pi \int_{\nu_1}^{\nu_2} \frac{c_1 \nu^3}{\exp(c_2 \nu/T) - 1} \, d\nu \tag{11}$$

where B_ν is the Planck intensity at wave number ν, $c_1 = 1.1909$ erg cm^{-2} sec^{-1} ster^{-1}, $c_2 = 1.4389$ cm deg^{-1}, and T is temperature. With the substitution $v = c_2 \nu / T$, Equation (11) becomes

$$B_r = \frac{\pi c_1 T^4}{c_2^4} \int_{v_1}^{v_2} \frac{v^3}{e^v - 1} \, dv. \tag{12}$$

Equation (12) can be written as

$$B_r = \frac{\pi c_1 T^4}{c_2^4} \int_0^{v_2} \frac{v^3}{e^v - 1} \, dv - \int_0^{v_1} \frac{v^3}{e^v - 1} \, dv \quad . \tag{13}$$

Pivovonsky and Nagel (ref. 9) give the following formulas for computing the integrals in Equation (13).

For $v \leq 3.5$,

$$\int_0^v \frac{v^3}{e^v - 1} \, dv \cong v^3 \left(\frac{1}{3} - \frac{v}{8} + \frac{v^2}{60} - \frac{v^4}{5040} + \frac{v^6}{272160} - \frac{v^8}{13,305,600} \right). \tag{14}$$

TABLE 1

CONSTANTS FOR INFRARED SPECTRAL INTERVALS

[From ref. 8]

Spectral Interval	Wave number Range $\nu(cm^{-1})$	CO_2			H_2O		
		m_r $(cm\ STP)^{-1}$	n_r	γ_r	m_r $(cm^2 g^{-1})$	n_r	γ_r
1	0 - 200	0.0	0.0	0	5.1×10^2	0.50	0
2	200 - 250	0.0	0.0	0	8.0×10^2	0.50	0
3	250 - 335	0.0	0.0	0	2.0×10^2	0.46	0
4	335 - 495	0.0	0.0	0	1.4×10^1	0.40	100
5	495 - 550	4.8×10^{-5}	0.65	1400	3.0	0.50	300
6	550 - 625	2.0×10^{-3}	0.38	800	1.0	0.50	400
7	625 - 660	5.8×10^{-1}	0.41	400	0.0	0.0	0
8	660 - 720	6.5×10^{-1}	0.37	600	0.0	0.0	0
9	720 - 810	9.6×10^{-4}	0.39	1000	0.0	0.0	0
10	810 - 880	5.1×10^{-5}	0.55	2800	0.0	0.0	0
11	880 - 920	3.2×10^{-7}	0.47	2040	0.0	0.0	0
12	920 - 1000	7.5×10^{-6}	0.47	2040	0.0	0.0	0
13	1000 - 1100	1.6×10^{-5}	0.51	1950	0.0	0.0	0
14	1100 - 1600	0.0	0.0	0	3.5×10^1	0.48	300
15	1600 - 2000	0.0	0.0	0	1.4×10^1	0.48	300
16	2000 - 2600	6.7×10^{-4}	0.22	0	0.0	0.0	0
17	2600 - 8000	1.6×10^{-6}	0.31	0	1.8	0.48	0

For $v \geq 3.5$,

$$\int_0^v \frac{v^3}{e^v - 1}\, dv \simeq \left\{ \frac{\pi^4}{15} - \sum_{m=1}^{3} e^{-mv}/m^4 \left[\left((mv + 3)mv + 6 \right) mv + 6 \right] \right\} \quad (15)$$

Equation (2) is integrated numerically by dividing the Venusian atmosphere into n layers of constant pressure thickness, each layer being 0.2 atmospheres thick.

ATMOSPHERIC MODEL

The atmospheric models used in the computations are based on the results of the Mariner 5 and Venera 4 spacecraft observations, and Earth-based spectroscopic and radiometric observations. Both the radio occultation experiment of Mariner 5 (ref. 10) and the direct sampling experiment of Venera 4 (ref. 1) indicate that the Venusian atmosphere is predominantly carbon dioxide - the Mariner 5 results suggesting 75 - to 90-percent CO_2, the Venera 4 results suggesting $\geq$ 90-percent CO_2. For the present calculations, we assume a 100-percent CO_2 atmosphere.

The spectroscopic determinations of H_2O concentrations (ref. 11-13) suggest water vapor mixing ratios of 10^{-4} to 10^{-5}. The direct observations of Venera 4, on the other hand, indicate H_2O mixing ratios of 1 to 7 x 10^{-3}. To cover the range of observed values, we shall perform computations for H_2O mixing ratios of 10^{-3}, 10^{-4}, and 10^{-5}.

A surface pressure of 20 atmospheres was measured by Venera 4 (ref. 1). There are indications that the Venera 4 observation does not refer to the surface of Venus (see, for example, ref. 4), and that the actual surface may be 20 km below the point at which Venera 4 measured 20 atm. In this case, the surface pressure of Venus would be about 65 atm, based upon an adiabatic extrapolation of the Mariner 5 results to the surface. We shall perform calculations for both surface pressures.

The lower atmosphere (tropospheric) lapse-rate deduced from the Venera 4 observations is $\sim 9\,^{\circ}K/km$ (ref. 15). The pressure at the tropopause level, as deduced from the temperature profile inferred from the Mariner 5 observations (ref. 10) is of the order of a few tenths of an atmosphere. This is also the pressure inferred for the vicinity of the cloud-top (ref. 16). In the present computations, a linear lapse-rate of $9\,^{\circ}K/km$ is assumed for the Venusian troposphere and an isothermal layer is assumed for the stratosphere. Computations are performed for different tropopause pressures - 0.2 atm, 0.4 atm, and 0.0 atm (no stratosphere) - and cloud pressures - 0.2 atm and 0.4 atm.

The characteristics of the model atmospheres used in the calculations are summarized in Table 2.

TABLE 2

CHARACTERISTICS OF MODEL ATMOSPHERES USED IN CALCULATIONS

Atmospheric Composition:	100% CO_2
Tropospheric lapse-rate:	$9^{\circ}K/km$
Tropopause pressure:	0.2 atm, 0.4 atm, 0.0 atm
Stratospheric lapse-rate:	Isothermal
H_2O mixing ratio:	10^{-3}, 10^{-4}, 10^{-5}
Surface pressure:	20 atm, 65 atm
Cloud infrared transmittance:	0.1, 0.5, 1.0 (clear skies)
Cloud pressure:	0.2 atm, 0.4 atm

TABLE 3

COMPUTED VENUSIAN SURFACE TEMPERATURES, T_s, AND TROPOPAUSE TEMPERATURES, T_{trop}, (°K), FOR DIFFERENT WATER VAPOR MIXING RATIOS, w, AND EFFECTIVE TEMPERATURES OF NET INCOMING SOLAR RADIATION, T_e

(100% CO_2 atmosphere; surface pressure, 20 atm; tropospheric lapse rate, 9°K/km; tropopause pressure, 0.2 atm)

T_e (°K)	w							
	10^{-3}		10^{-4}		10^{-5}		0	
	T_s	T_{trop}	T_s	T_{trop}	T_s	T_{trop}	T_s	T_{trop}
237	520	213	482	197	420	172	282	115
336	757	310	682	278	583	238		

RESULTS

Calculations with surface pressure of 20 atm. - A series of greenhouse computations was performed to evaluate the effect of H_2O vapor on the computed surface temperature. These computations were performed for two effective temperatures of the net incoming solar radiation, T_e = 237°K and T_e = 336°K. The former represents the mean planetary value averaged over the Venusian year while the latter is representative of insolation conditions at the sub-solar point on Venus. Both are based upon an albedo of 0.73. The computations are for a 100-percent CO_2 atmosphere, surface pressure of 20 atm, tropospheric lapse-rate of 9°K/km, and no clouds. The tropopause is assumed to be located at a pressure level of 0.2 atm. The computed surface and tropopause temperatures are shown in Table 3.

For the case of no water vapor (w = 0), in which the greenhouse effect is due solely to carbon dioxide, the computed surface temperature is only 282°K. The addition of only a small concentration of water vapor, 10^{-5}, is sufficient to raise the mean surface temperature to 420°K. Best agreement with the Venera 4 data, which indicated a surface temperature of 543°K on the night side, close to the equator and about 1500 km from the terminator, is obtained with an H_2O mixing ratio of 10^{-3}. However, the computed temperature of 520°K is below the mean planetary surface temperatures of 600°K to 700°K obtained from microwave observations and inferred from Mariner 5. Thus, if the water vapor mixing ratio is 10^{-3}, the greenhouse effect due to CO_2 and H_2O can produce a mean surface temperature in agreement with the Venera 4 observations but still below the probable mean surface temperature of 600°K to 700°K. Water vapor mixing ratios of 10^{-4} and 10^{-5} yield mean temperatures less than 500°K, which are definitely lower than those observed.

The effect of varying the pressure at the tropopause level is shown in Table 4. Lowering the tropopause decreases the computed surface temperatures; raising it increases the surface temperature. The effect is greatest at the higher water vapor concentrations. If the tropopause is at a pressure greater than 0.4 atm, even the presence of a water vapor mixing ratio of 10^{-3} could not produce a greenhouse surface temperature greater than 500°K.

Thus far the effect of the cloud layer has not been included. The pressure at the Venusian cloud top is believed to be of the order of a few tenths of an atmosphere. We have performed calculations for cloud top pressures of 0.2 atm and 0.4 atm, and infrared cloud transmittances of 0.5 and 0.1. The computed surface temperatures are plotted versus cloud transmittance in Figures 3 through 6.

TABLE 4

COMPUTED VENUSIAN SURFACE TEMPERATURES, T_s, AND TROPOPAUSE TEMPERATURES, T_{trop}, (^oK), FOR DIFFERENT WATER VAPOR MIXING RATIOS, w, AND TROPOPAUSE PRESSURE LEVELS, p_{trop}

(100% CO_2 atmosphere; surface pressure, 20 atm; tropospheric lapse rate, $9^oK/km$; $T_e = 237^oK$)

p_{trop} (atm)	w					
	10^{-3}		10^{-4}		10^{-5}	
	T_s	T_{trop}	T_s	T_{trop}	T_s	T_{trop}
0.4	482	226	461	215	412	193
0.2	520	213	482	197	420	172
0.0	539	0	490	0	421	0

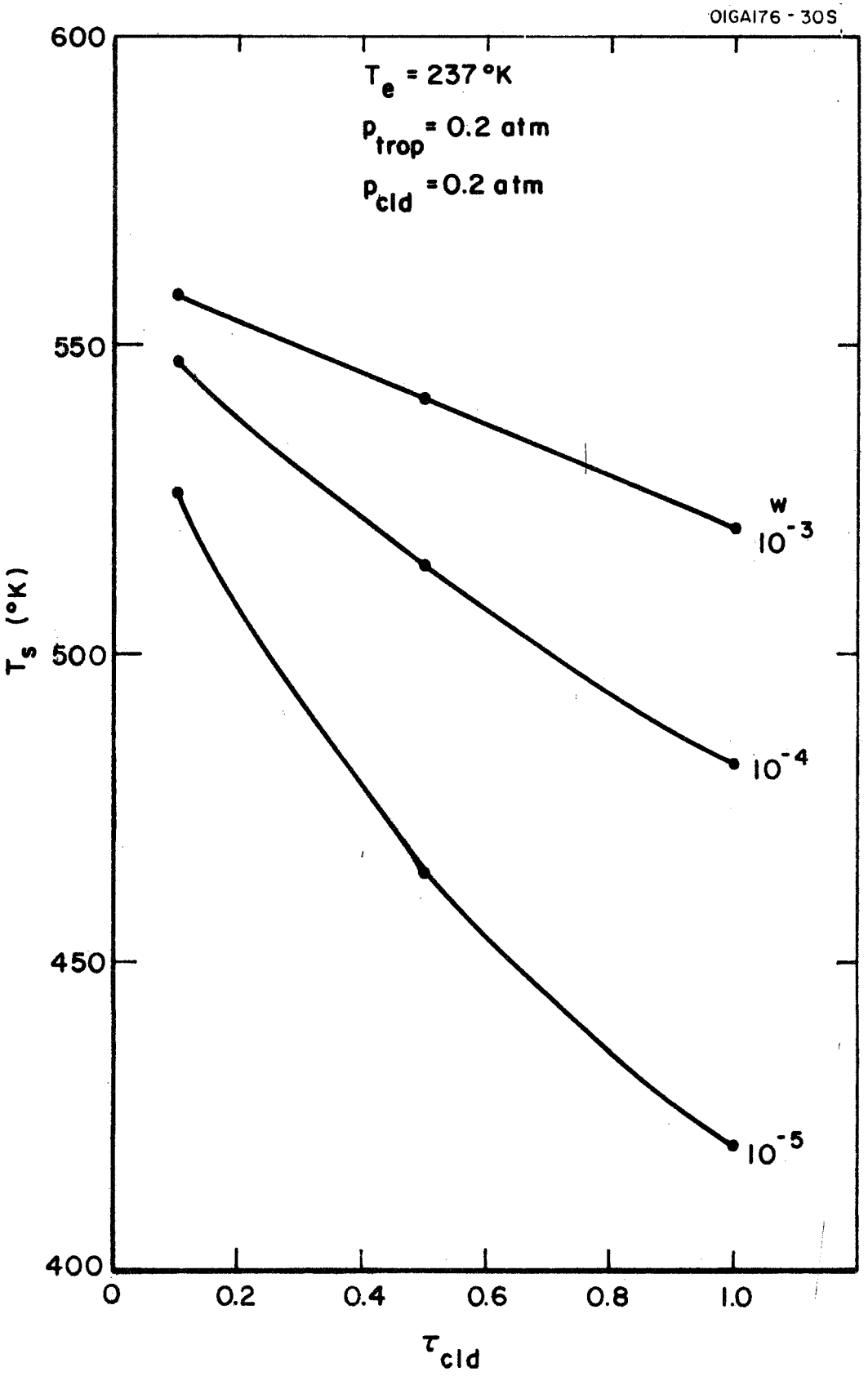

Figure 3. Variation of computed Venusian surface temperature with assumed infrared transmittance of cloud layer. (w is H_2O mixing ratio; 100% CO_2 atmosphere; surface pressure = 20 atm; tropospheric lapse rate = 9^oK/km)

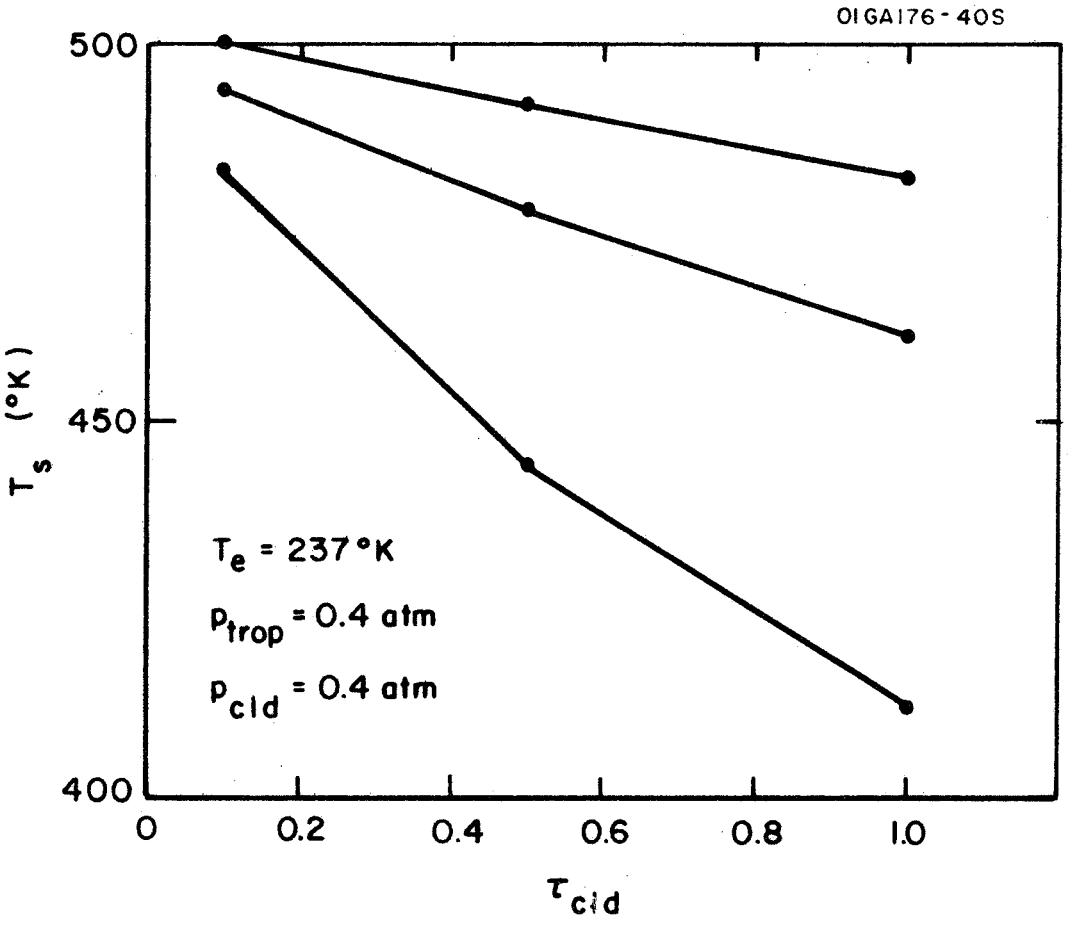

Figure 4. Variation of computed Venusian surface temperature with assumed infrared transmittance of cloud layer. (w is H_2O mixing ratio; 100% CO_2 atmosphere; surface pressure = 20 atm; tropospheric lapse rate = 9^oK/km.)

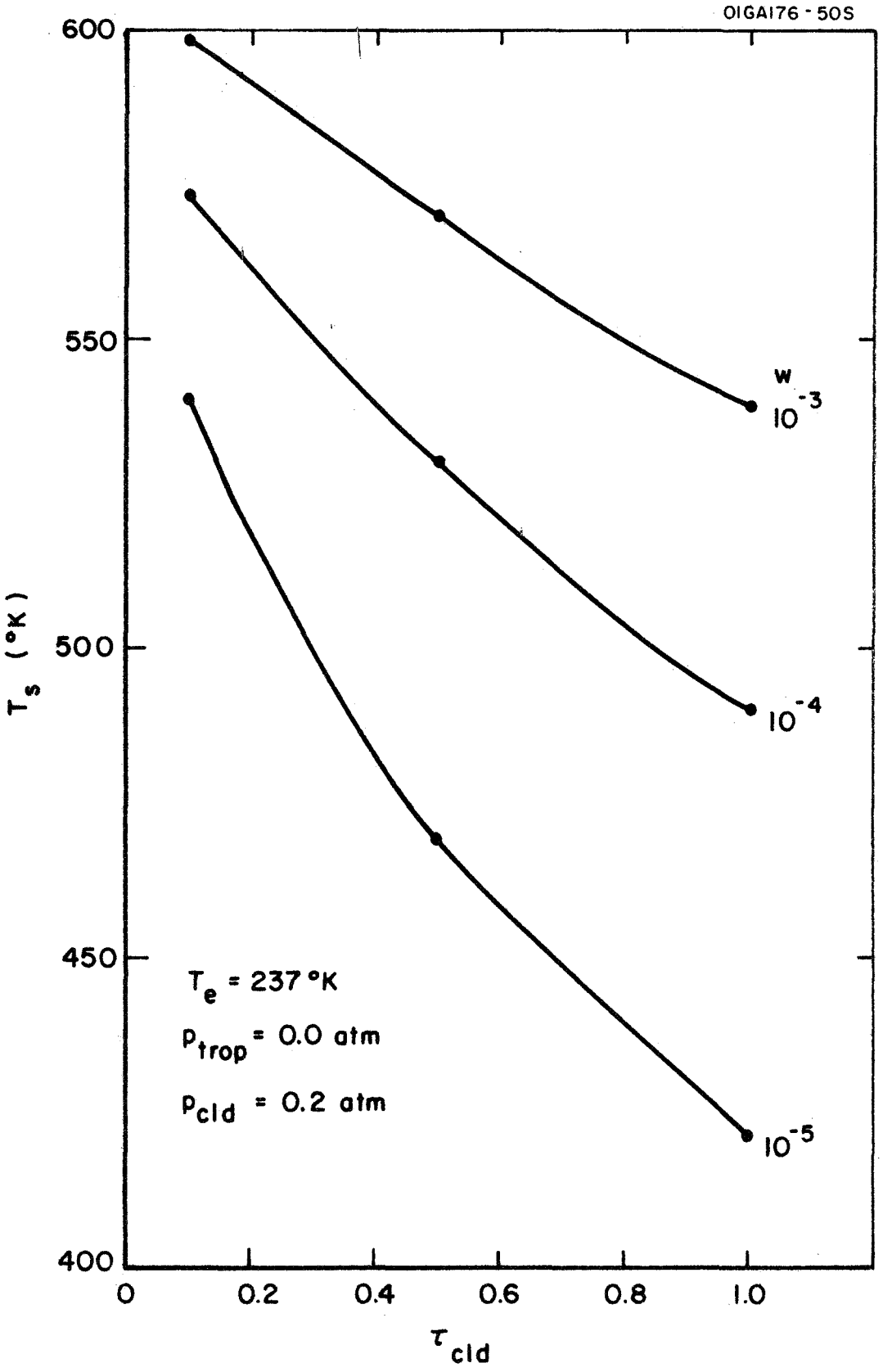

Figure 5. Variation of computed Venusian surface temperature with assumed infrared transmittance of cloud layer. (w is H_2O mixing ratio; 100% CO_2 atmosphere; surface pressure = 20 atm; tropospheric lapse rate = 9°K.km.)

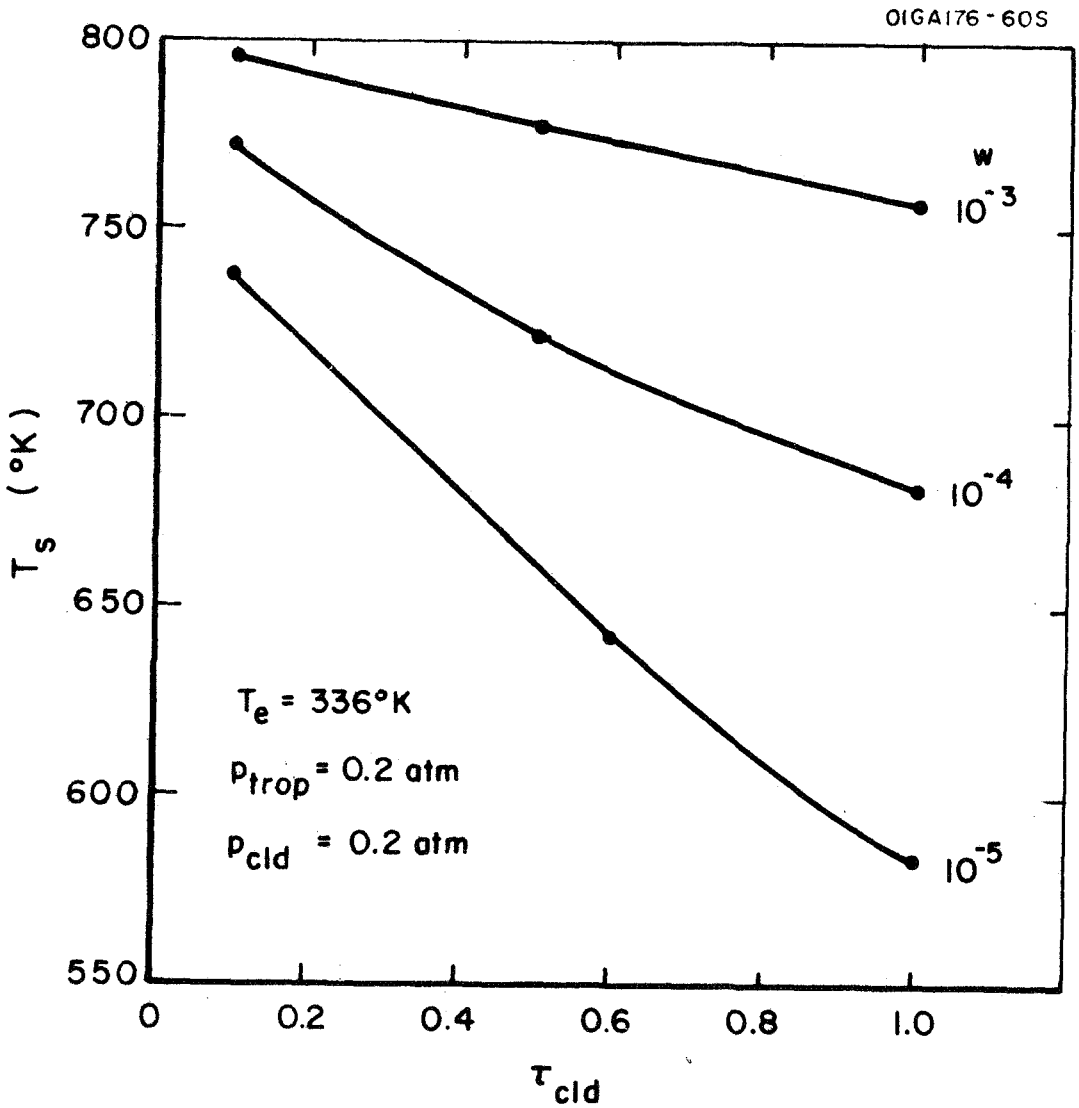

Figure 6. Variation of computed Venusian surface temperature with assumed infrared transmittance of cloud layer. (w is H_2O mixing ratio; 100% CO_2 atmosphere; surface pressure = 20 atm; tropospheric lapse rate = 9°K/km.)

The values for a cloud transmittance of 1.0 correspond to the cases of clear skies discussed earlier. The effect of an infrared absorbing cloud on the computed surface temperature is obvious. For example, from Figure 3 it can be seen that with an H_2O mixing ratio of 10^{-5} the computed surface temperature increases from 420°K for clear skies to 525°K for a cloud with infrared transmittance of 0.1.

In general the results for the 20 atmosphere surface pressure model indicate that mean surface temperatures between 500°K and 600°K can be maintained by the atmospheric greenhouse effect if the water vapor mixing ratios are of the order of 10^{-3}, as measured by Venera 4. If the water vapor mixing ratios are of the order 10^{-4} or 10^{-5}, mean surface temperatures greater than 500°K can be maintained only if the infrared transmittance of the cloud is a few tenths or less. Mean surface temperatures of 600°K to 700°K cannot be attained; even with the highest H_2O concentration, 10^{-3}, and lowest infrared cloud transmittance, 0.1.

Calculations with surface pressure of 65 atm. - The deeper 65 atmosphere model produces a greater greenhouse effect. The results of calculations for assumed tropopause and cloud pressures of 0.2 atm are shown in Figure 7 for three different water vapor concentrations. If clouds do not contribute to the greenhouse effect ($\tau_{cld} = 1.0$), a surface temperature of greater than 650°K can be maintained only if the water vapor mixing ratio is 10^{-3} or greater. If clouds contribute to the greenhouse effect, then surface temperatures of >650°K can be maintained with lower water vapor concentrations. These calculations are all for the case of average net incoming solar radiation (effective temperature, T_e, of 237°K), tropospheric lapse-rate of 9°C/km, 100% CO_2 atmosphere and surface pressure of 65 atm.

The effect of raising the assumed tropopause and cloud pressures to 0.4 atm is shown in Figure 8. The computed surface temperatures are 15°K to 80°K lower than for the corresponding calculations of Figure 7. None of the computed surface temperatures are greater than 650°K, the highest computed value being 630°K for an H_2O mixing ratio of 10^{-3} and an infrared cloud transmittance of 0.1.

The results for a surface pressure of 65 atm may be compared with the previous results for 20 atm. The increase by a factor of more than three in total atmosphere causes an increase in the magnitude of the greenhouse effect such that the surface temperatures run about 25% higher.

A set of computations was performed to evaluate the effect of a completely dry atmosphere. The results are shown in Table 5. The case of $\tau_{cld} = 1.0$ corresponds to a cloudless atmosphere in which the entire weight of the greenhouse effect is carried by carbon dioxide alone. The computed surface temperature in this case is only 285°K. As a cloud with increasing infrared opacity (decreasing transmittance) is introduced,

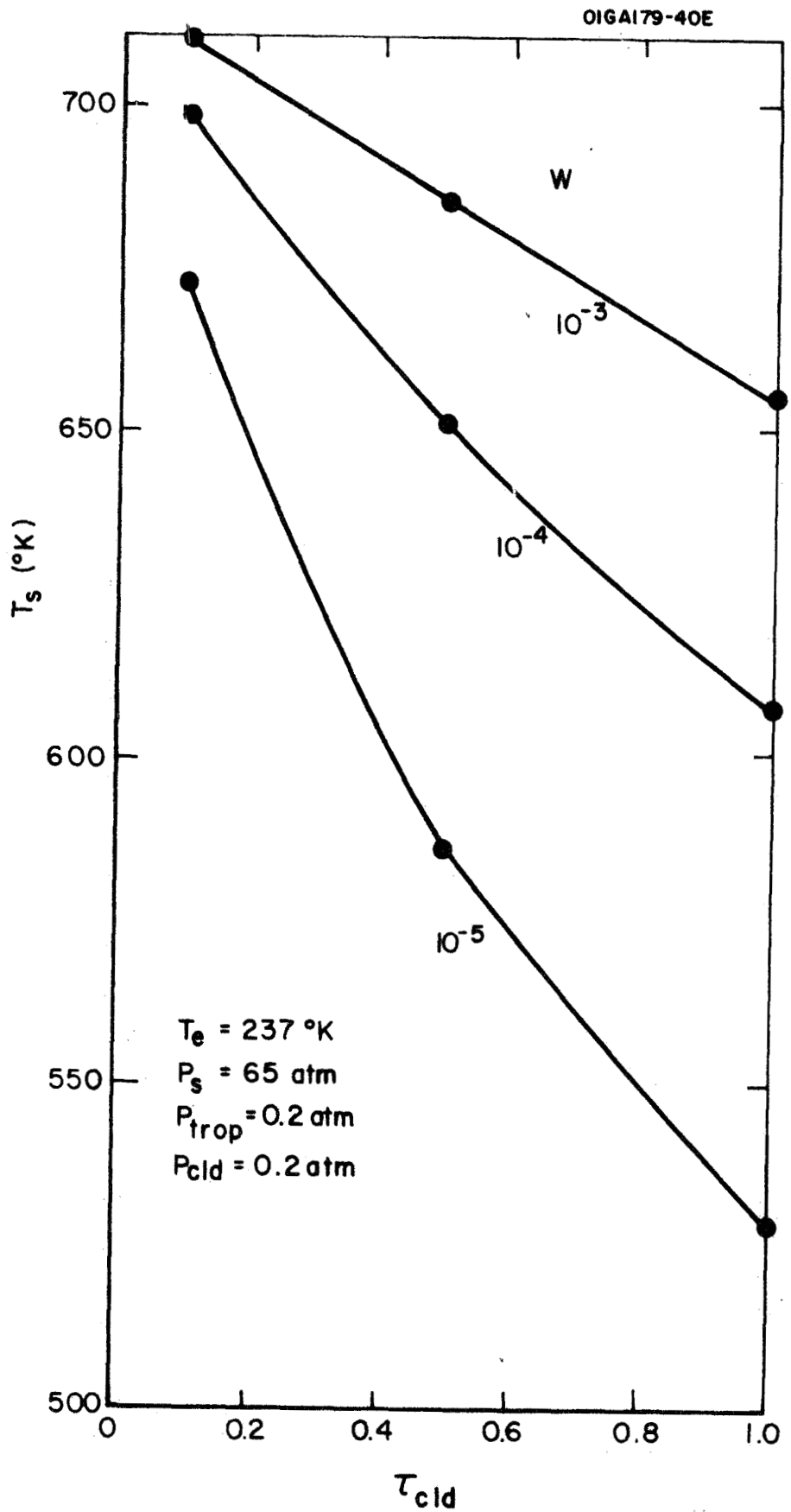

Figure 7. Variation of computed Venusian surface temperature with assumed infrared transmittance of cloud layer.

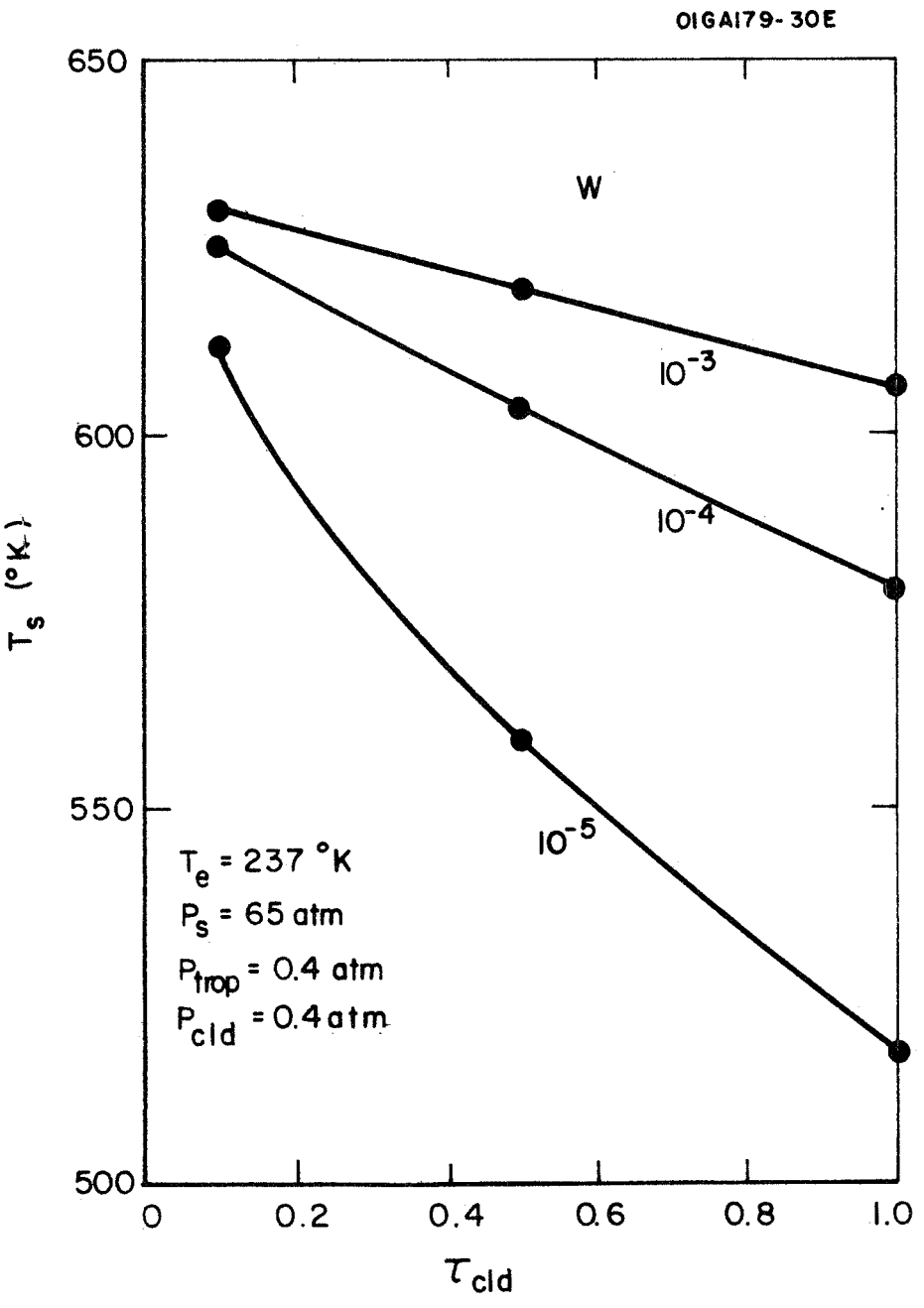

Figure 8. Variation of computed Venusian surface temperature with assumed infrared transmittance of cloud layer.

TABLE 5

COMPUTED VENUSIAN SURFACE TEMPERATURES (^{o}K)
IN THE ABSENCE OF ATMOSPHERIC WATER VAPOR
FOR DIFFERENT CLOUD TRANSMITTANCES

(100% CO_2 atmosphere; surface pressure, 65 atm;
tropospheric lapse-rate, 9^{o}K/km; tropopause pressure, 0.2 atm;
cloud pressure, 0.2 atm; T_e = 237^{o}K)

τ_{cld}	T_s
1.0	285
0.5	336
0.1	474

the computed surface temperature increases to a value of 474°K for τ_{cld} = 0.1.

Another set of computations was performed to evaluate a greenhouse effect produced by water vapor alone - that is, in the absence of atmospheric carbon dioxide. The computed surface temperatures are shown in Table 6. As the water vapor mixing ratio varies over two orders of magnitude - from 10^{-3} to 10^{-5} - the surface temperature changes only 7°K, from 294°K to 287°K.

As a partial test of the technique, the model was applied to Earth and Mars. For Earth, the actual mean surface temperature is known, of course, and for Mars, the mean surface temperature can be reliably estimated from available theoretical and observational results. Although the parameters that go into the models - such as tropopause pressure, cloud pressure, tropospheric lapse rate, etc. - are better known for Earth, and even for Mars, than for Venus, a comparison of computed with actual surface temperatures gives some indication of the validity of the model. The results of these calculations are shown in Table 7, in which the input parameters are listed in the upper half of the table and the results in the lower half. The input parameters of the column labeled b are representative of average conditions of cloudiness and albedo on Earth. A 100% cloud cover with infrared transmittance of 0.5 is assumed at a pressure of 500 mb. Radiatively, this is equivalent to the observed average of 50% cloudiness with infrared cloud transmittance of 0.0 (black body). The computed mean surface temperature is 301°K; the observed mean surface temperature is 288°K. Column a input parameters include the effect of the clouds on the albedo, as in column b, but not on the infrared emission - that is, the infrared transmittance of the clouds is assumed equal to 1.0. In this case, the computed surface temperature drops 9°K. Column c assumes an Earth with clear skies. The computed surface temperature is 313°K. The computation for Mars, which yields a surface temperature of 212°K, is in good agreement with observed indications of, and more elaborate computations of, the mean surface temperature (see, for example, ref. 5).

Another test of the technique can be performed by comparing our computed emission spectrum with available observations of the Venusian emission spectrum. The Venusian emission spectrum between 750 cm^{-1} and 1200 cm^{-1} has recently been observed by Hanel, et al (ref.17). In Figure 9 we compare the recent observations with our computed emission spectrum for the case of surface pressure = 65 atm; water vapor mixing ratio = 10^{-3}; 100% carbon dioxide atmosphere; infrared cloud transmittance = 0.1; tropopause and cloud pressures of 0.2 atm; effective temperature of net incoming solar radiation = 237°K; tropospheric lapse rate 9°C/km. This case yields a surface temperature (710°K) and tropopause temperature (232°K) most nearly in agreement with the observational indications of surface and tropopause temperature on Venus. Hanel, et al's (ref. 17)

TABLE 6

COMPUTED VENUSIAN SURFACE TEMPERATURES (^{o}K) IN THE ABSENCE OF ATMOSPHERIC CARBON DIOXIDE AND CLOUDS FOR DIFFERENT WATER VAPOR MIXING RATIOS, w

(Surface pressure, 65 atm; tropospheric lapse-rate, 9^{o}K/km; tropopause pressure, 0.2 atm)

w	T_s
10^{-3}	294
10^{-4}	292
10^{-5}	287

TABLE 7

GREENHOUSE MODEL APPLIED TO EARTH AND MARS

(Input parameters are listed in upper part of table; computed surface and tropopause temperatures in lower part)

	EARTH			MARS
	a	b	c	
p_s (mb)		1000		5
H_2O (by mass)		2.0×10^{-3}		0
CO_2 (by mass)		4.5×10^{-4}		1.0
dT/dz (^oC/km)		6.5		5.1
p_{trop} (mb)		200		2.5
p_{cld} (mb)		500		-
τ_{cld}	1.0	0.5	1.0	-
Albedo	0.35	0.35	0.15	0.30
T_e (^oK)	252	252	270	208
T_s (^oK)	292	301	313	212
T_{trop} (^oK)	206	222	230	177

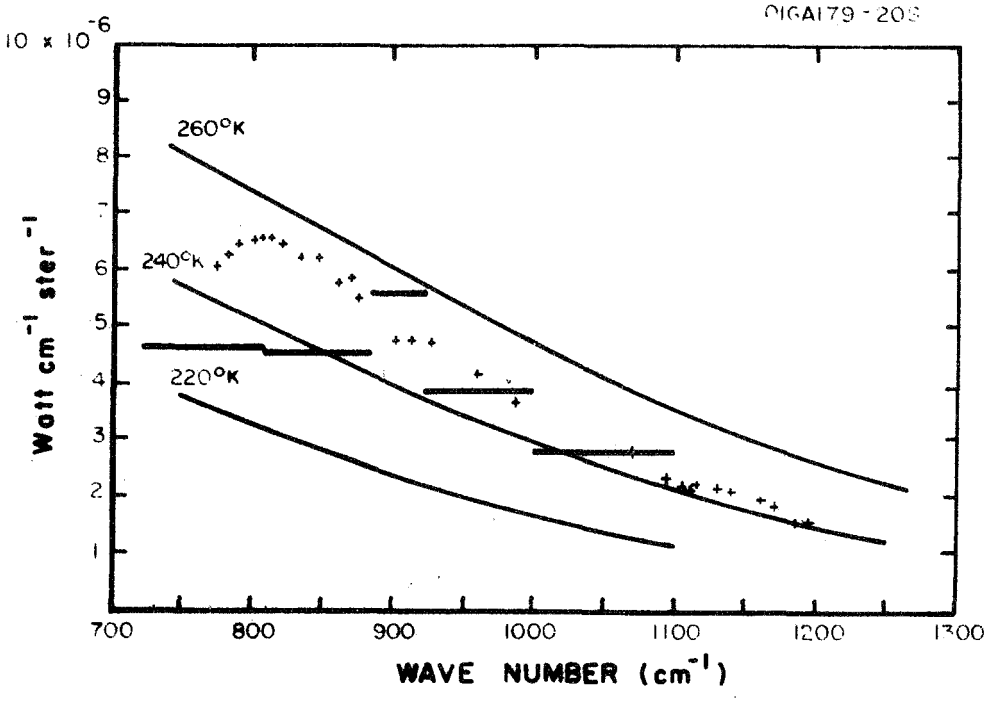

Figure 9. Comparison of computed Venusian emission spectrum (horizontal bars) with observed spectrum (ref. 17) (+ + + + +) between 8 and 12μ. Curves represent black-body emission temperatures. Computations are for model atmosphere of 100% CO_2; surface pressure, 65 atm; H_2O mixing ratio, 10^{-3}; infrared cloud transmittance, 0.1; tropospheric lapse rate, 9°C/km; effective temperature of net incoming solar radiation, 237°K.

observations indicate an emission temperature of ~ 250°K compared to Sinton and Strong's (ref. 18) observations of 225°K to 230°K. The agreement between the calculated and the observed spectra is fairly good. Although not shown on the graph, our computed emission in the 1100 to 1600 cm^{-1} region of 0.89 watts cm^{-1} $ster^{-1}$ corresponds to an emission temperature of 240°K, in good agreement with Hanel et al's values between 1100 and 1200 cm^{-1}.

Other observations of the emission of Venus in this spectral region have been made (ref. 19-21). These observers report emission temperatures of 200 to 225°K - lower than the 225°K to 230°K observed by Sinton and Strong (ref. 18) and much lower than the 250°K observed by Hanel et al. (ref. 17). These lower emission temperatures would not be consistent with our calculated emission spectrum.

Discussion and Conclusions. - The observational indications of surface temperature - the microwave observations and extrapolation of the Mariner 5 and Venera 4 results to the radar observed radius of the planet - suggest a mean surface temperature for Venus of about 700°K. The average solar radiation available to heat the planet and its atmosphere - after albedo losses - has an equivalent temperature of about 237°K. In the absence of a greenhouse effect, this would be the value of the surface temperature. This short wavelength solar energy is distributed to the surface and atmosphere by radiative and dynamical processes. Energy in an amount equal to that received from the sun is radiated back to space in the form of long wavelength thermal radiation. In the greenhouse model of the present study, we have assumed that the shape or form of the vertical temperature profile of the Venus atmosphere is known from the Mariner 5 and Venera 4 observations. For a variety of model atmospheres, we then computed the surface temperatures that led to a balance of net incoming solar radiation and emerging thermal radiation. The results indicate that mean surface temperatures of 650°K to 700°K can be maintained by the greenhouse mechanism if the surface pressure is ~ 65 atm and if water vapor mixing ratios are of the order of 10^{-3} or, in the event the water vapor content is lower, if the clouds are moderately opaque to infrared radiation. These requirements and the other characteristics of the model atmosphere used in the calculations are in good agreement with observational indications of the Venusian atmosphere. Thus, we may conclude that an efficient atmospheric greenhouse due to large amounts of CO_2, moderate amounts of H_2O, a surface pressure of ~ 65 atm, and a cloud layer with moderate infrared transmittance (~ 0.1) is most probably responsible for the high surface temperature on the planet Venus. If the infrared transmittance of the cloud is lower than ~ 0.1, if there is a large amount of particulate matter in the Venusian atmosphere that absorbs infrared radiation (see ref. 6), or if collision - induced transitions add to the infrared opacity of the Venusian atmosphere (ref. 22), the water vapor requirement becomes even less stringent.

It is of interest to compare the results of the present non-grey computations with results based upon the use of grey models. Calculations with grey models (ref. 3 and 5) indicate that an atmospheric infrared opacity of 40 to 60 is required to maintain a surface temperature of 600°K. The required opacity can be translated to a required transmittance by means of the formula

$$\tau = 2 E_3(x)$$

where E_3 is the third exponential integral and x is the required opacity.[3] An opacity greater than 40 corresponds to transmittances less than 10^{-19}. It was on the basis of such a small allowable fraction of surface radiation penetrating to space that arguments were presented against the greenhouse mechanism as the explanation of the high surface temperature. We can compare the transmittance for the non-grey calculations with the above value. In the non-grey calculations, the infrared transmittance of the atmosphere is simply the fraction of the surface radiation that escapes to space. The infrared transmittances required of the non-grey atmosphere to produce surface temperatures of ~ 600°K are orders of magnitude lower than those required in the grey case. For example, a transmittance of 10^{-6} is required to produce a surface temperature of ~ 600°K in the model atmosphere with surface pressure 65 atm and H_2O mixing ratio of 10^{-4}. These results suggest that it may be dangerous to use a grey model to infer the allowable infrared transmittance of a deep, absorbing atmosphere, given its surface temperature. The inferred transmittance may differ quite considerably from the actual non-grey transmittance.

It is interesting to note that it takes <u>both</u> CO_2 and H_2O to produce the large greenhouse effect. One without the other would produce surface temperatures of only ~ 300°K. The reason for this is that each gas has windows in the infrared spectrum. But together, in the quantities observed on Venus, they blanket the infrared spectrum.

REFERENCES

1. Avduevsky, V.S., M. Ya. Marov, and M. Rozhdestvensky, 1968: Model of the atmosphere of Venus based on results of measurements made by the Soviet automatic interplanetary station Venera 4. J. of Atmos. Sci., 25, 537-545.

2. Sagan, C., 1960: The radiation balance of Venus. Jet Prop. Lab. Tech. Report 32-34, 23 pp.

3. Jastrow, R., and S. I. Rasool, 1963: Radiative transfer in the atmospheres of Venus and Mars. In Space Research, v. 3, Wiley, New York, 1036-1041.

4. Ostriker, J.P., 1963: Radiative transfer in a finite grey atmosphere. Astrophys. J., 138, 281-290.

5. Ohring, G., and J. Mariano, 1964: The effect of cloudiness on a greenhouse model of the Venus atmosphere. J. Geophys. Res., 69, 165-175.

6. Samuelson, R.A., 1967: Greenhouse effect in semi-infinite scattering atmospheres: Application to Venus. Astrophys. J., 147, 782-798.

7. Burch, D., D. Gryvnak, E. Singleton, W. France, and D. Williams, 1962: Infrared absorption by carbon dioxide, water vapor, and minor atmospheric constituents. AFCRL-62-698, 316 pp.

8. Bartko, F., and R. Hanel, 1968: Non-gray equilibrium temperature distributions above the clouds of Venus. Astrophys. J., 151, 365-378.

9. Pivovonsky, M., and M. Nagel, 1961: Tables of Blackbody Radiation Functions, MacMillan, New York, 481 pp.

10. Kliore, A., G. Levy, D. Cain, G. Fjeldbo, and S. Rasool, 1967: Atmosphere and ionosphere of Venus from the Mariner V S-band radio occultation measurement. Science, 158, 1683-1688.

11. Dollfus, A., 1963: Observation of water vapor on the planet Venus. Compt. Rend., 256, 3250-3253.

12. Bottema, M., et al., 1965: A quantitative measurement of water vapor in the atmosphere of Venus. Ann. Astrophys., 28, 225-228.

13. Belton, M., R. Goody, and D. Hunten, 1967: Quantitative spectroscopy of Venus in the region 8000-11000Å. Kitt Peak National Observatory Contribution No. 241.

14. Jastrow, R., 1968: The planet Venus. Science, 160, 1403-1410.

15. Anderson, A. D., 1968: Superadiabatic layer on Venus, as inferred from the Venera-4 probe measurements. Nature, 217, 627-628.

16. Belton, M., D. Hunten, and R. Goody, 1968: Quantitative spectroscopy of Venus in the region 8,000-11,000Å. In The Atmospheres of Mars and Venus, ed. J. Brandt and M. McElroy, Gordon and Breach, N.Y. 69-98.

17. Hanel, R., M. Forman, and G. Stamback, 1968: Preliminary results of Venus observations between 8 and 13 microns. J. Atmos. Sci., 25, 586-593.

18. Sinton, W., and J. Strong, 1960: Radiometric observations of Venus. Astrophys. J., 131, 470-490.

19. Murray, B., R. Wildey, and J. Westphal, 1963: Infrared photometric mapping of Venus through the 8- to 14-micron atmospheric window. J. Geophys. Res., 68, 4813-4818.

20. Westphal, J., R. Wildey, and B. Murray, 1965: The 8-14 micron appearance of Venus before the 1964 conjunction. Astrophy. J., 142, 799-902.

21. Gillett, F., F. Low, and W. Stein, 1968: Absolute spectrum of Venus from 2.8 to 14 microns. J. Atmos. Sci., 25, 594-595.

22. Solomon, P., 1968: Opacity of the Venus atmosphere. In Infrared Astronomy, ed. P. Brancazio and A. Cameron, Gordon and Breach, New York, 171-180

PART 2

MEAN VERTICAL TEMPERATURE PROFILE OF VENUSIAN ATMOSPHERE: THEORETICAL CALCULATIONS BASED UPON RADIATIVE EQUILIBRIUM

George Ohring

MEAN VERTICAL TEMPERATURE PROFILE OF VENUSIAN ATMOSPHERE: THEORETICAL CALCULATIONS BASED UPON RADIATIVE EQUILIBRIUM

ABSTRACT

Mean radiative equilibrium temperature profiles are calculated for the Venusian atmosphere. It is assumed that the equilibrium is the result of gaseous absorption and emission, and a non-grey transmittance model is used. The equilibrium temperatures are computed with an iteration technique. The assumed model atmosphere consists of 100% carbon dioxide with a trace - 10^{-5} - of water vapor. Calculations are performed for two surface pressure models - 20 atm and 65 atm. For the 20 atm model, the computed radiative equilibrium surface temperature is 490°K; for the 65 atm model, 676°K. The radiative equilibrium temperature profile for the 65 atm model is in general agreement with the observational indications of the Venusian temperature profile.

INTRODUCTION

The first observational indications of the vertical temperature profile of the Venusian atmosphere are based upon the measurements of Mariner 5 and Venera 4, and are shown in Figure 1 (after ref. 1). They indicate that the temperature decreases with altitude at a lapse-rate of about $9^{\circ}K/km$ to an altitude of about 60 km, above which it remains approximately constant at about $250^{\circ}K$. The temperature profile below the level reached by Venera 4 is uncertain, as indicated by the dotted extrapolation lines. Two interesting features of the observed profile are: 1) the lapse-rate of $9^{\circ}K/km$, which is approximately equal to the adiabatic lapse rate, and 2) the approximately isothermal region capping the lower atmosphere. Both are typical of a temperature profile produced by radiative and convective processes, suggesting that theoretical calculations of the vertical temperature structure with a radiative-convective model should be quite useful for studies of the Venusian thermal structure. In the present study we develop a non-grey radiative equilibrium model and perform calculations of the mean radiative equilibrium temperature profile in the Venusian atmosphere.

Radiative equilibrium temperature profiles have been calculated previously for Venus (ref. 2-5). Mintz (ref. 2), and Hanel and Bartko (ref. 3) confined their calculations to the region above the cloud layer (cloud top pressure taken as a few tenths of an atmosphere). Jastrow and Rasool (ref. 4) used the Eddington approximation for a grey atmosphere, while Samuelson's calculations (ref. 5) were based upon radiative equilibrium in a particulate medium. In none of the previous work is a non-grey radiative model used to calculate the temperature profile of the entire atmosphere. The present computations use a non-grey infrared transmittance model and are based upon atmospheric compositions and surface pressures derived mainly from the recent Mariner 5 and Venera 4 observations.

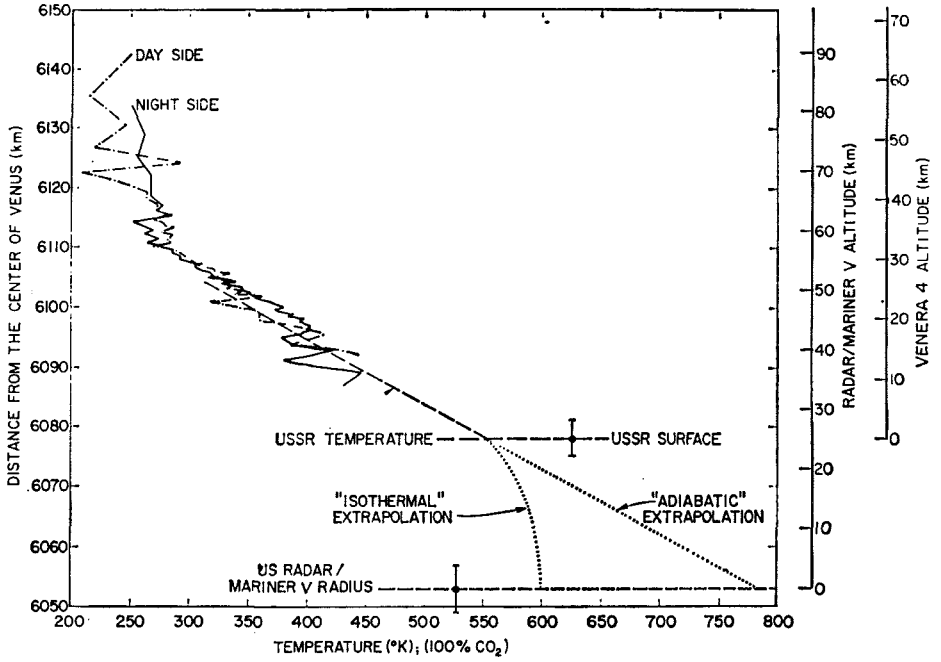

Figure 1. Temperature profiles determined by Mariner 5 and Venera 4, and extrapolations to the level of the mean surface (After ref. 1).

RADIATIVE EQUILIBRIUM MODEL

In the present model, we assume that radiative equilibrium is established as a result of gaseous absorption and emission. (The effect of clouds and particulates will be introduced in later models.) The upward and downward infrared fluxes of radiation at a level i in a spectral interval r can be written as

$$F_r(i)\uparrow = B_r(s)\ \tau_r(i,s) + \int_{\tau_r(i,s)}^{1} B_r\, d\tau_r \qquad (1)$$

$$F_r(i)\downarrow = \int_{\tau_r(i,N)}^{1} B_r\, d\tau_r \qquad (2)$$

where B_r is the black-body flux in the spectral interval, τ_r is the flux transmittance of the spectral interval, s refers to the planet's surface, N to the top of the atmosphere. $\tau_r(i,s)$ represents the transmittance of the layer between the surface and level i; $\tau_r(i,N)$ represents the transmittance between the top of the atmosphere and level i. The total infrared flux at level i, $F_{net}(i)$, is obtained by summing (1) and (2) over all spectral intervals and subtracting the downward flux from the upward flux.

$$F_{net}(i) = \sum_r F_r(i)\uparrow - \sum_r F_r(i)\downarrow \qquad (3)$$

The solar radiation intensity at level i in the spectral interval r is given by

$$I_r(i) = I_r(N) \cdot \cos\ \zeta \cdot \tau_r(i,N) \cdot (1-A) \qquad (4)$$

where $I_r(N)$ is the solar radiation intensity in spectral interval r at the top of the atmosphere, ζ is the zenith angle of the sun, and A is the planetary albedo. $\tau_r(i,N)$ in the solar radiation calculation is computed for the slant path. The total intensity of solar radiation at i, I(i), is obtained by summing over all intervals of the solar spectrum.

$$I(i) = \sum_r I_r(i) \qquad (5)$$

In radiative equilibrium, the net infrared flux balances the solar radiation intensity at each level in the atmosphere.

$$F_{net}(i) = I(i) \tag{6}$$

This implies that the radiative rate of temperature change at each level is equal to zero.

$$\frac{dT}{dt} = \frac{g}{c_p} \frac{d}{dp} [F_{net} - I] \tag{7}$$

where g is the gravitational acceleration, p is pressure, and c_p is the specific heat at constant pressure.

The problem is to determine the temperature profile that satisfies Equations (6) and (7).

Initially, we used the time marching method of computing radiative equilibrium temperatures (ref. 6). The computational procedure is quite simple. An initial temperature profile is assumed. Radiative rates of temperature change for all layers are computed from the finite difference analog of (7). These rates are applied for a time step Δt to obtain new temperatures for the atmospheric layers. The new surface temperature is computed from the radiative balance at the planetary surface

$$\sigma T_s^4 = F(s)\downarrow + I(s) \tag{8}$$

The process is repeated until the radiative rates of temperature change are negligibly small. We found, however, that this procedure was inefficient. A small time step was required to keep the computations stable and this resulted in an inordinately large number of iterations to arrive at the final temperature profile. Various smoothing measures increased the stability of the computations, but the process remained basically inefficient. As a result, another method for computing radiative equilibrium temperatures was derived, tested, and adopted for the calculations. This method is described below.

The solar radiation flux at each level, I(i), is not a function of temperature (except for a minor effect due to the temperature dependence of the transmittance) and can thus be computed once and for all for a particular solar zenith angle, albedo, and atmospheric composition and

pressures. At equilibrium, $F_{net}(i)$ must equal I(i), as shown in Equation (6). Thus, we know the equilibrium values of $F_{net}(i)$. From this information, we would like to determine the equilibrium temperatures T(i). We can arrive at the equilibrium temperature profile T(i) by an iterative process that corrects the temperatures until equilibrium is reached. We start with an assumed temperature profile $T^n(i)$, where n represents the nth iteration and compute $F^n_{net}(i)$. We assume, for our correction procedure, that the net infrared flux at the level i is due mainly to the radiation fluxes emitted by the layers adjacent to i, and, further, that the emission is proportional to the fourth power of the temperature. Thus, for our correction procedure, we assume

$$F_{net}(i) \sim \left[T(i)^4 - T(i+1)^4\right] \tag{9}$$

where the index i, when used with temperature, refers to the temperature of the layer immediately below the level i. This assumption leads to the following correction procedures

$$\left(T^{n+1}_{(N)}\right)^4 = \left(T^{n}_{(N)}\right)^4 \times \left[I(N)/F^{n}(i)\right] \tag{10}$$

and

$$\left(T^{n+1}_{(i)}\right)^4 = \left(T^{n+1}_{(i+1)}\right)^4 + \left[\left(T^{n}_{(i)}\right)^4 - \left(T^{n}_{(i+1)}\right)^4\right] \times \left[I(i)/F^{n}_{net}(i)\right] \tag{11}$$

A new temperature at iteration (n+1) at the top layer, N, of the atmosphere, is computed from correction Equation (10). New temperatures at iteration (n+1) at successive lower layers i in the atmosphere are computed from correction Equation (11). The entire process is repeated until the difference between the net infrared flux and the solar flux at each level is less than a fraction ϵ of the solar flux at that level.

$$\frac{F_{net}(i) - I(i)}{I(i)} \leq \epsilon \tag{12}$$

This new iteration scheme has proven to be extremely stable and provides rapid convergence to the equilibrium temperature profile.

Although the assumed dependence of net infrared flux on temperature in the correction procedure is basically valid only for optically thick, grey atmospheres, the scheme has also worked well when applied to Earth and Mars, as will be shown later.

TRANSMITTANCE AND ATMOSPHERIC MODELS

Absorption and emission by carbon dioxide and water vapor are considered in the calculations. We adopt the same transmittance model as was used in Part 1 of this technical report, which is based upon the Bartko and Hanel (ref. 3) strong line fits to available laboratory and theoretical transmittance data. In this model, the wavenumber range 0-8000 cm^{-1} is divided into 17 spectral intervals. Absorption of solar radiation takes place in spectral interval 16 (2000-2600 cm^{-1}) and spectral interval 17 (2600-8000 cm^{-1}). At wavenumbers greater than 8000 cm^{-1}, it is assumed that no solar energy is absorbed in the atmosphere. All seventeen spectral intervals contribute to the infrared emission.

The model atmosphere is assumed to be composed of 100% CO_2 with an H_2O mixing ratio of 10^{-5}. Calculations are performed for two surface pressures - 20 atm and 65 atm. The former is based upon the hypothesis that Venera reached the surface of Venus, the latter upon the hypothesis that it did not (see, for example, ref. 7).

RESULTS

The radiative transfer equations are integrated numerically by dividing the atmosphere up into a number of layers at constant pressure thickness. Several computations were performed to determine the minimum number of layers required to yield reasonably accurate estimates of the surface temperature and vertical temperature profile. These computations were performed for an atmospheric model with surface pressure of 20 atm and water vapor mixing ratio of 10^{-5}. The solar zenith angle was taken as 45^{o}, which would make the resulting temperature profile typical of the average day-side equatorial region. The number of layers was varied from 10 to 80, the corresponding pressure thickness of each layer from 2 to 0.25 atm. Table 1 contains a list of the input parameters and the computed surface temperature for these (Exps. 100 to 103) and other experiments conducted during the study. In this Table, p_s is the surface pressure, CO_2 and H_2O are the relative CO_2 and H_2O concentrations, ζ is the solar zenith angle, N is the number of atmospheric layers used in the integration of the radiative transfer equations, Δp is the pressure thickness of each atmospheric layer, ϵ is the convergence criterion, and T_s is the computed surface temperature.

TABLE 1

PARAMETERS AND COMPUTED SURFACE TEMPERATURES OF RADIATIVE EQUILIBRIUM EXPERIMENTS

Exp.No.	p_s (atm)	CO_2	H_2O	$\cos\zeta$	N	Δp (atm)	ϵ (%)	T_s (^{o}K)
100	20	1.0	10^{-5}	0.707	20	1	1	555
101	20	1.0	10^{-5}	0.707	10	2	1	503
102	20	1.0	10^{-5}	0.707	40	0.5	1	591
103	20	1.0	10^{-5}	0.707	80	0.25	1	608
104	20	1.0	10^{-5}	0.25	80	0.25	1	489
105	65	1.0	10^{-5}	0.25	80	0.8125	1	618
106	65	1.0	10^{-5}	0.25	160	0.4062	1	676
Mars 1	0.01	1.0	3.73×10^{-5}	0.25	40	2.5×10^{-4}	1	216
Earth 1	1	4.5×10^{-4}	3×10^{-3}	0.25	40	2.5×10^{-2}	1	312

The computed surface temperatures increase from 503°K to 608°K as the number of layers increases from 10 to 80. The reason for this centers around the large amounts of absorbing gas - particularly CO_2, but also H_2O - in each layer. Layers 2 atm, 1 atm, and even 0.5 atm are optically thick. Thus, an error is made in the integration of the radiative transfer equation if one divides the atmosphere into such layers for purposes of numerical integration. For example, the downward flux of infrared radiation at the surface is given by

$$F(s)\downarrow = \sum_r \int_{\tau_r(s,N)}^{1} B_r(T)\,d\tau_r \qquad (13)$$

If the temperature profile is isothermal it is obvious that no matter how many layers are used to evaluate the integral in Equation (13), the answer will be the same. However, if there is a temperature lapse rate, and if the atmosphere is optically thick in the infrared, then the computed value of the integral will be in error, if the number of layers used is too small. Qualitatively, this can be seen by the following argument. Suppose one is dealing with an atmosphere in which a layer of 1 atmosphere thickness is optically thick (say, less than 1% infrared transmittance). This implies that 99% of the contribution to the downward infrared flux of radiation at the surface would come from the first layer of 1 atm thickness adjacent to the surface. If one divides such an atmosphere into layers of 2 atm thickness to evaluate Equation (13), the downward flux at the surface would now be dependent upon the first layer of 2 atm thickness adjacent to the surface. If the temperature decreases with altitude, the downward flux would be lower for the computation with Δp = 2 atm than for the case with Δp = 1 atm.

This is essentially what is happening in our computations for Venus. For the higher values of Δp, the downward flux at the surface is being underestimated. Since the downward flux of infrared energy is a dominant factor in the surface energy budget on Venus, the surface temperature is underestimated.

Figure 2 shows a plot of the computed surface temperature versus the number of layers. This graph suggests that further increase in the number of layers beyond 80, or Δp below 0.25 atm, would not substantially change the computed surface temperature.

One should be able to fix the value of Δp to be used for such integrations by examining the integrated infrared transmittance as a function of Δp. Table 2 shows such integrated transmittances for atmospheric layers containing 100% CO_2, water vapor mixing ratio of 10^{-5}, pressure of 20 atm, and temperature of 500°K. They are computed from

$$\tau = \left[\sum_r \tau_r B_r(T) \right] / \sigma T^4 \qquad (14)$$

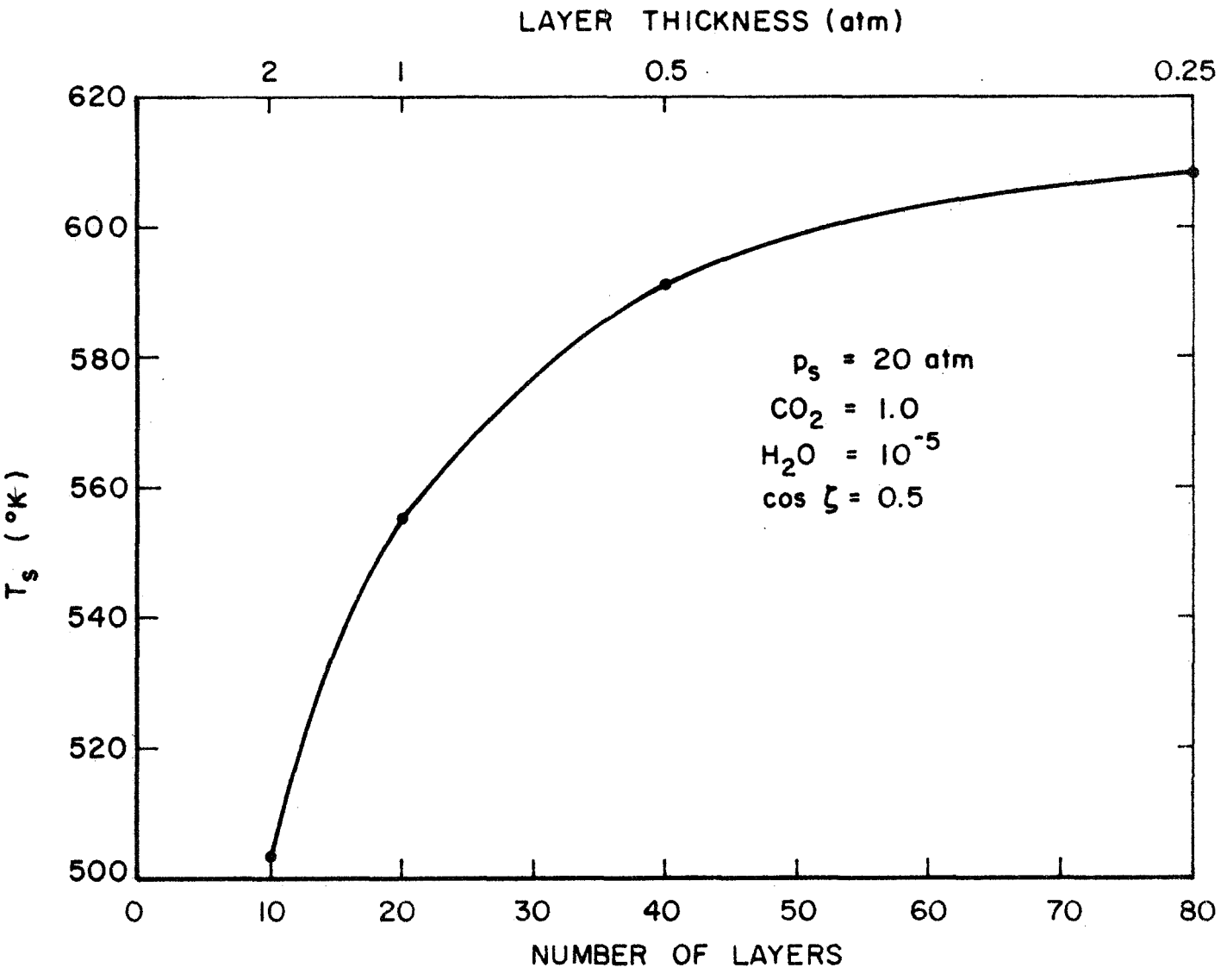

Figure 2. Computed Venusian surface temperature as a function of number of layers used in the numerical integration of the radiative transfer equation.

TABLE 2

INTEGRATED INFRARED TRANSMITTANCE (τ) FOR DIFFERENT PRESSURE THICKNESSES (Δp)

(CO_2 = 1.0, H_2O = 10^{-5}, p = 20 atm, T = 500°K)

Δp (atm)	τ
0.2	0.20
0.4	0.13
0.6	0.10
0.8	0.083
1.0	0.069
1.4	0.051
1.8	0.040
2.2	0.032
2.6	0.027
3.0	0.022

Table 2, taken together with the conclusion drawn from Figure 2, suggests that the integrated transmittance of each layer should be about .10 or more for reasonably accurate (within 5%) calculations of the radiative equilibrium temperature of the Venusian surface.

The complete vertical temperature profiles for these four cases are plotted in Figure 3. It can be seen that the temperatures converge in the upper layers, indicating that the major errors resulting from too small a value of N are confined to the surface and lower atmosphere temperatures.

We may take the N = 80 temperature profile as the radiative equilibrium temperature profile for this case. The radiative equilibrium temperature profile is unstable (lapse rate greater than adiabatic lapse rate) in the lower atmosphere. Convection would take place, resulting in a modified temperature profile. Nevertheless, it is interesting to note the high surface temperature (600°K) that would prevail in pure radiative equilibrium due to gaseous absorption and emission on Venus.

Figure 4 shows the radiative equilibrium temperature profile computed for $\cos \zeta = 0.25$. This value of $\cos\zeta$ would represent the average planetary insolation conditions; thus, the computed temperatures can be thought of as a mean Venusian radiative equilibrium temperature profile. The computed surface temperature of 490°K is well below the observed average surface temperatures of 650°K to 700°K.

Calculations with a surface pressure of 65 atm are shown in Figure 5. Analysis of integrated infrared transmittances indicates that at a temperature of 700°K and pressure of 65 atm, a transmittance of 0.10 occurs for a layer of thickness $\Delta p \approx 0.4$ atm. The number of layers, 160, used in this calculation insures that no layer has an integrated transmittance less than 0.10. The computed surface temperature is then within 5% of the surface temperature that would be computed with an infinite number of layers. In contrast to the 20 atm case, the computed surface temperature of 676°K is close to the observed mean surface temperature of Venus. Also plotted in Figure 5 is the temperature profile observed by Mariner 5/Venera 4, extrapolated to the probable surface (after ref. 7). The Mariner 5/Venera 4 profile is approximately in adiabatic equilibrium up to 0.2 atm. The shape of the computed radiative equilibrium profile is quite similar to the observed profile. The radiative equilibrium profile is superadiabatic in the lower atmosphere and the radiative equilibrium temperatures are more than 100°K lower than the observed temperatures in the middle atmosphere. However, the close agreement between the observed and computed profile is encouraging and suggests that the radiative processes considered in the present model do predominate on Venus.

It is of interest to compare the present non-grey radiative equilibrium temperature profile with those computed for a grey atmosphere.

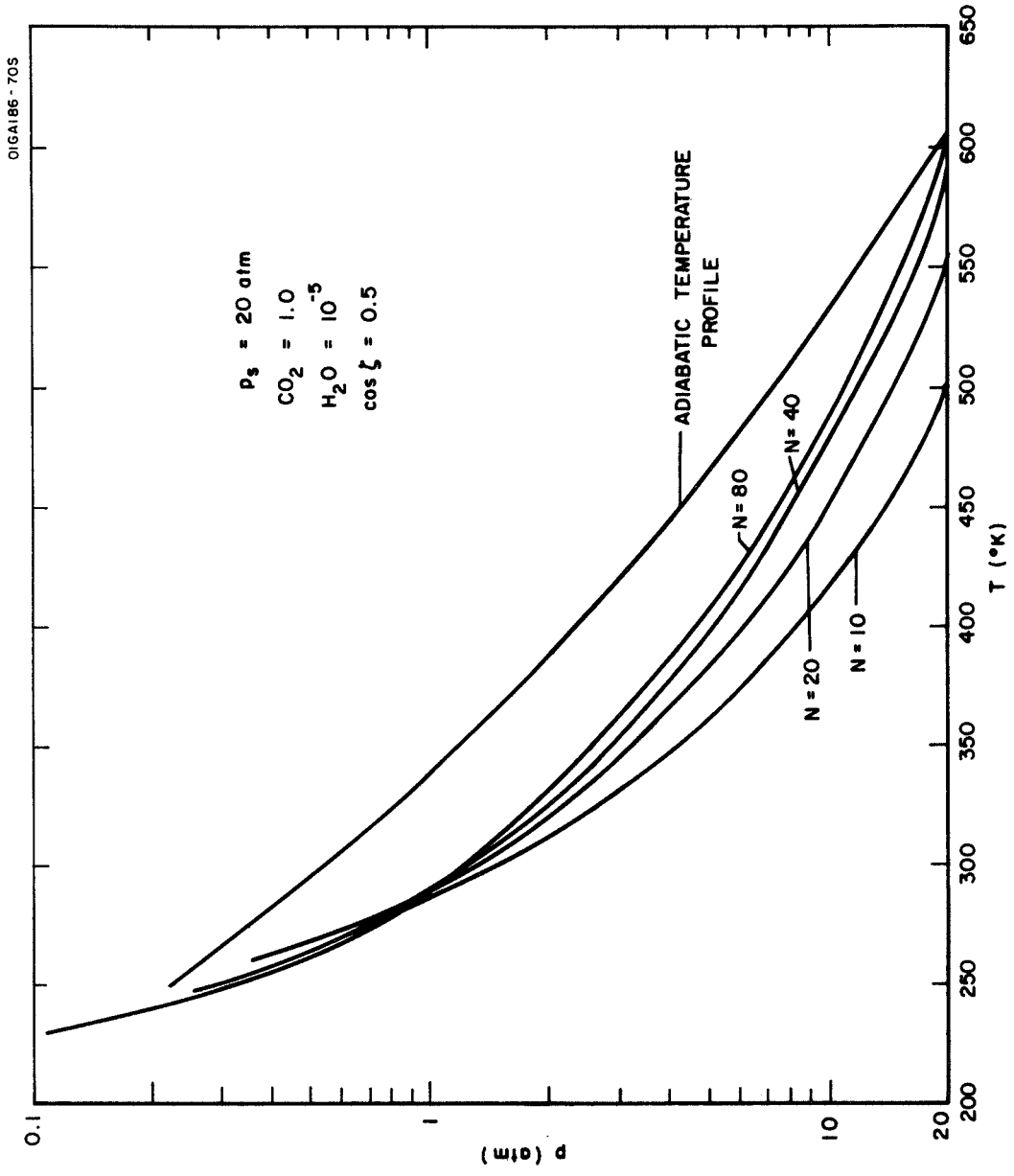

Figure 3. Radiative equilibrium temperature profiles for different values of N, the number of layers in the numerical integration of the radiative transfer equation.

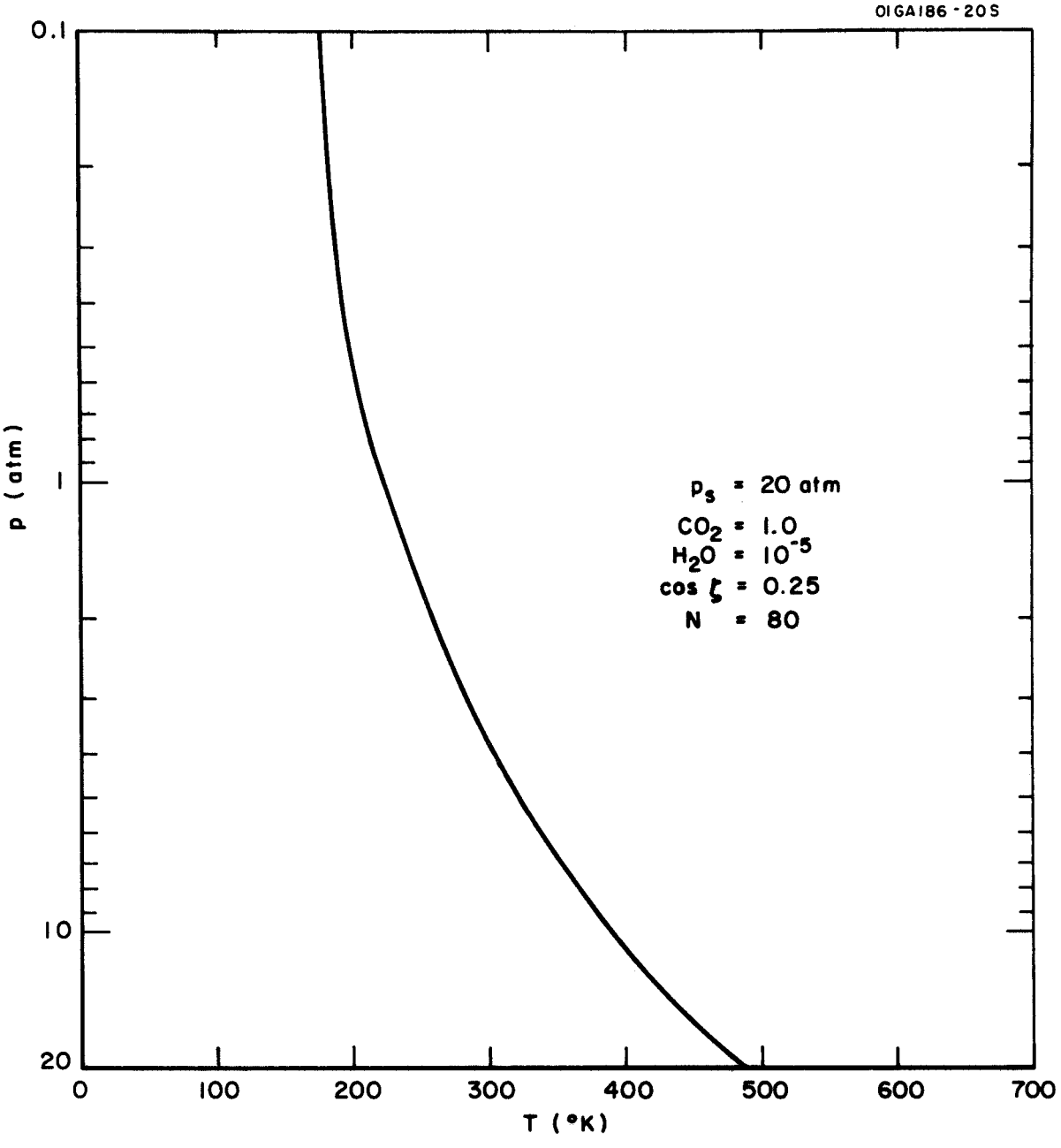

Figure 4. Mean radiative equilibrium temperature profile for Venus for surface pressure of 20 atm.

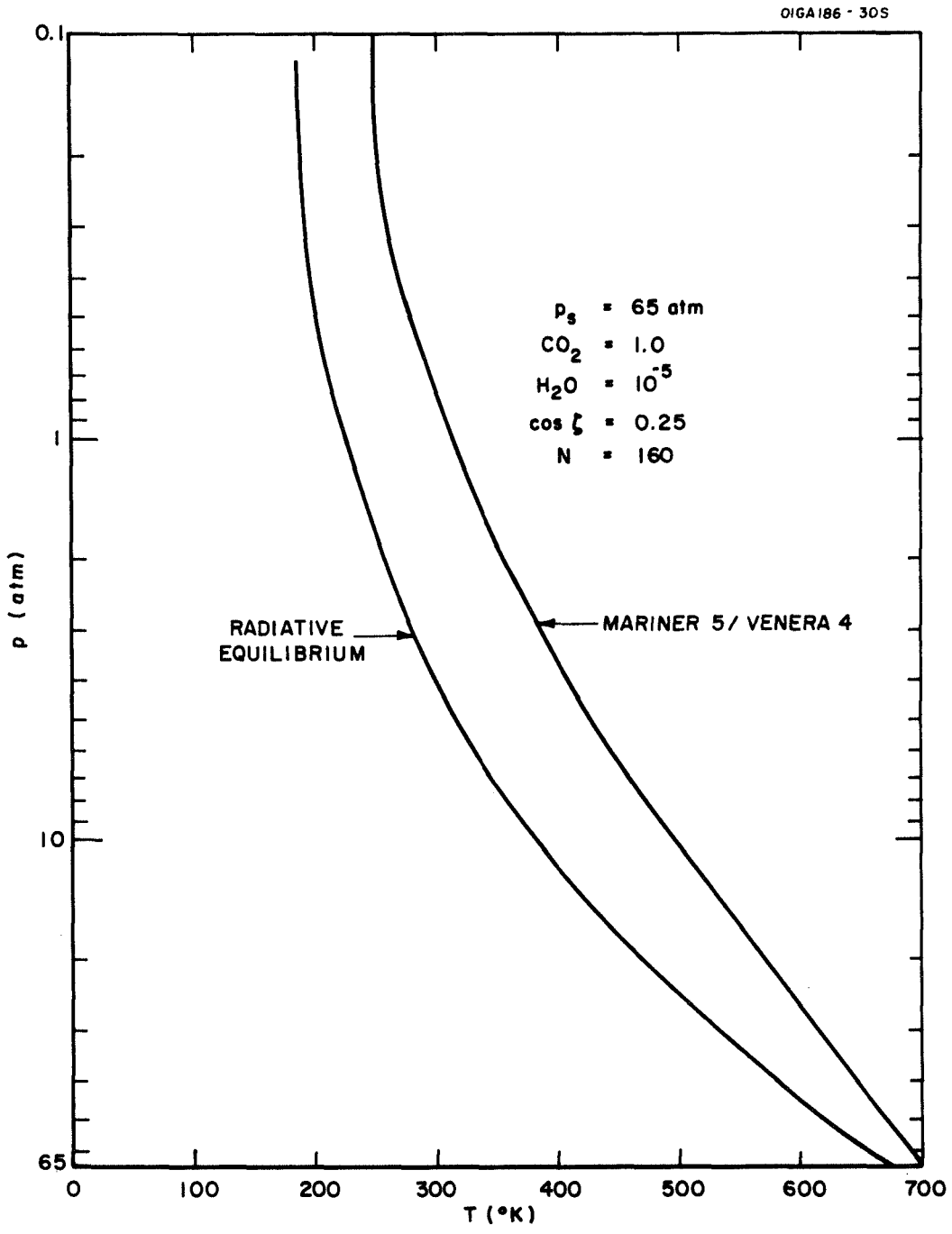

Figure 5. Mean radiative equilibrium temperature profile for Venus for surface pressure of 65 atm compared with observed temperature profile.

The Eddington approximation leads to the following formulas for temperature as a function of infrared opacity, X, and effective temperature of the net incoming solar radiation, T_e.

$$T(s) = T_e \left[1 + 0.75\, X(s)\right]^{0.25} \tag{14}$$

$$T(p) = T_e \left[0.5 + 0.75\, X(p)\right]^{0.25} \tag{15}$$

In Equation (14), T(s) is the surface temperature and X(s) is the total infrared opacity of the atmosphere. In Equation (15), T(p) and X(p) represent the temperature and infrared opacity as functions of pressure. Two methods have been used in the past to determine the value of X(s). In the first method, an estimate of the infrared transmittance, $\tau(s)$, of the atmosphere is obtained from its expected composition and surface pressure. This is converted to an opacity with the use of the relation

$$\tau(s) = 2E_3\, [X(s)], \tag{16}$$

where E_3 is the third exponential integral. In the second method, X(s) is assumed to be that value computed from Equation (14) that yields the observed surface temperature on Venus. In Figure 6 we compare our non-grey computation of the mean radiative equilibrium temperature profile for Venus with grey calculations using both methods. For the first method, we obtain our estimate of the total infrared transmittance of the atmosphere from the fraction of the surface radiation that escapes to space in our non-grey calculation, 1×10^{-5}. This corresponds to an infrared opacity of about 10. For the second method, we obtain an infrared opacity of 87 computed from Equation (14) for $T_e = 237^{\circ}K$ (mean planetary insolation) and $T(s) = 676^{\circ}K$, the result of our non-grey calculation. To evaluate Equation (15), we assume, in both cases, that the infrared opacity is directly proportional to pressure. It is quite obvious that the first method (infrared opacity = 10) grossly underestimates the surface temperature. The grey atmosphere profile that is essentially calibrated by our computed surface temperature (infrared opacity = 87) is in reasonable agreement with the non-grey calculation.

As a partial check of the method, and as a test of the iteration technique in optically thin atmospheres, mean radiative equilibrium temperature profiles were computed for Earth and Mars. Forty layers were used for the calculations in both atmospheres, and the results are plotted in Figures 7 and 8. The H_2O mixing ratio for Earth was chosen to yield a precipitable water vapor content of about 3 cm. The

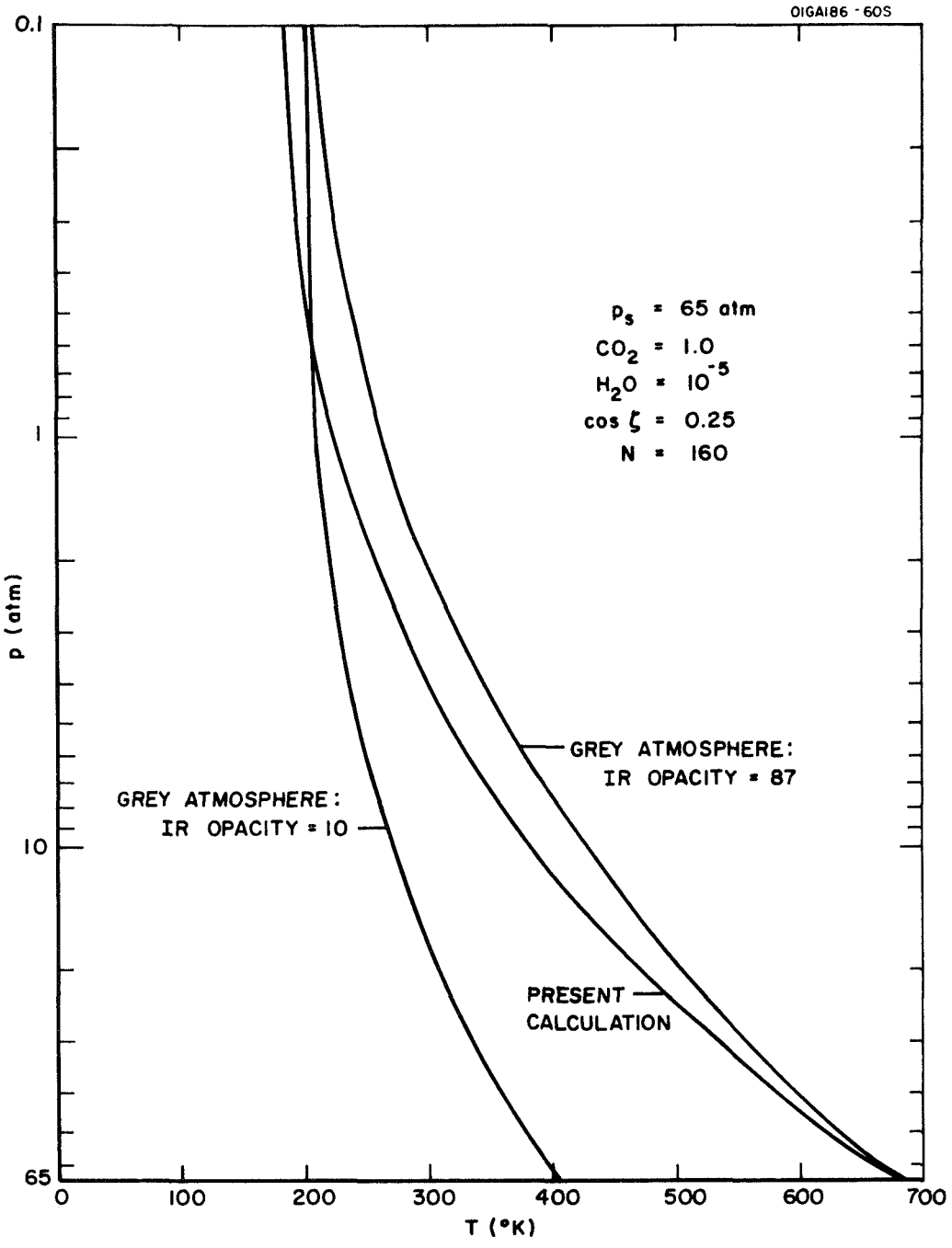

Figure 6. Mean radiative equilibrium temperature profile for Venus for surface pressure of 65 atm compared with two gray atmosphere profiles.

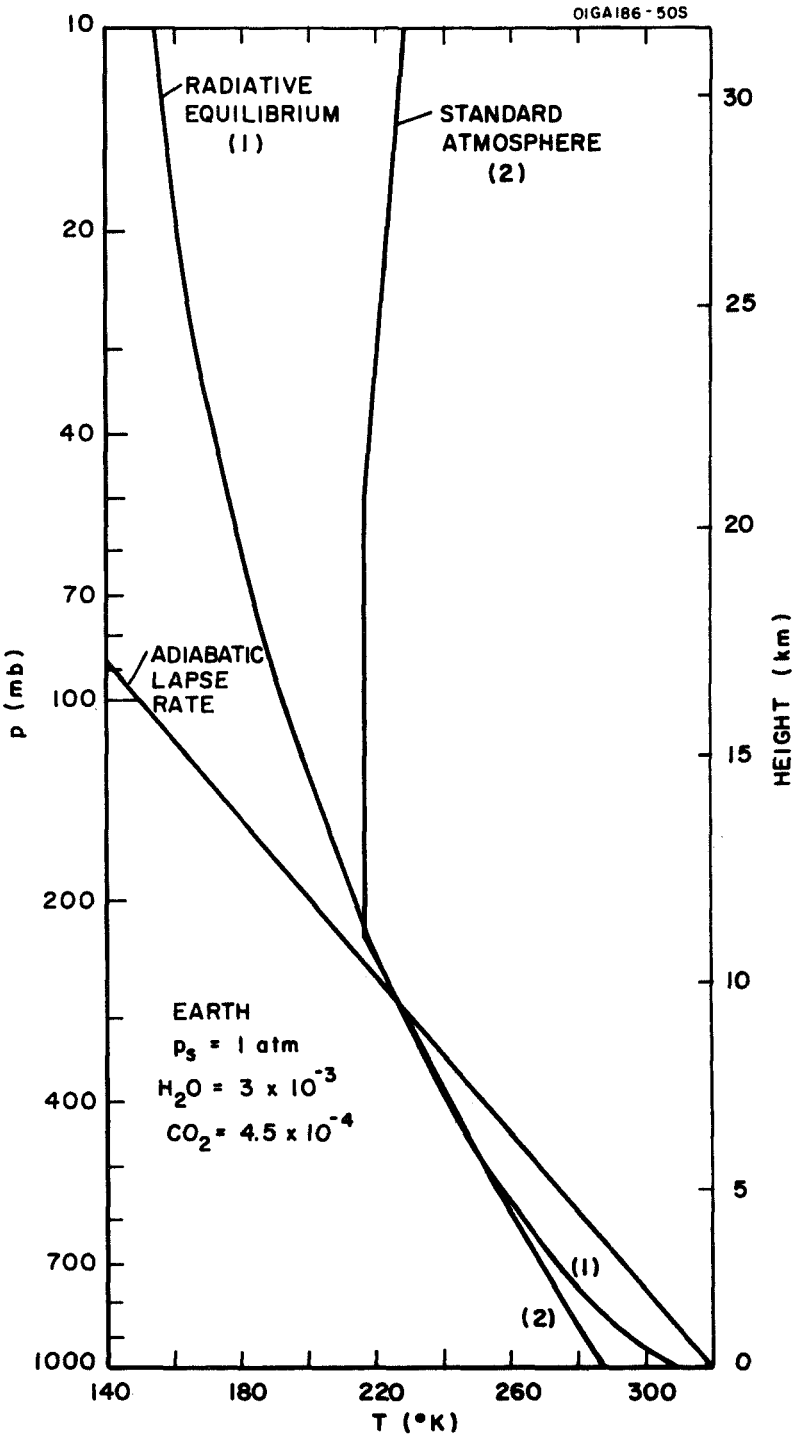

Figure 7. Mean radiative equilibrium temperature profile for Earth compared with standard atmosphere and adiabatic temperature profiles.

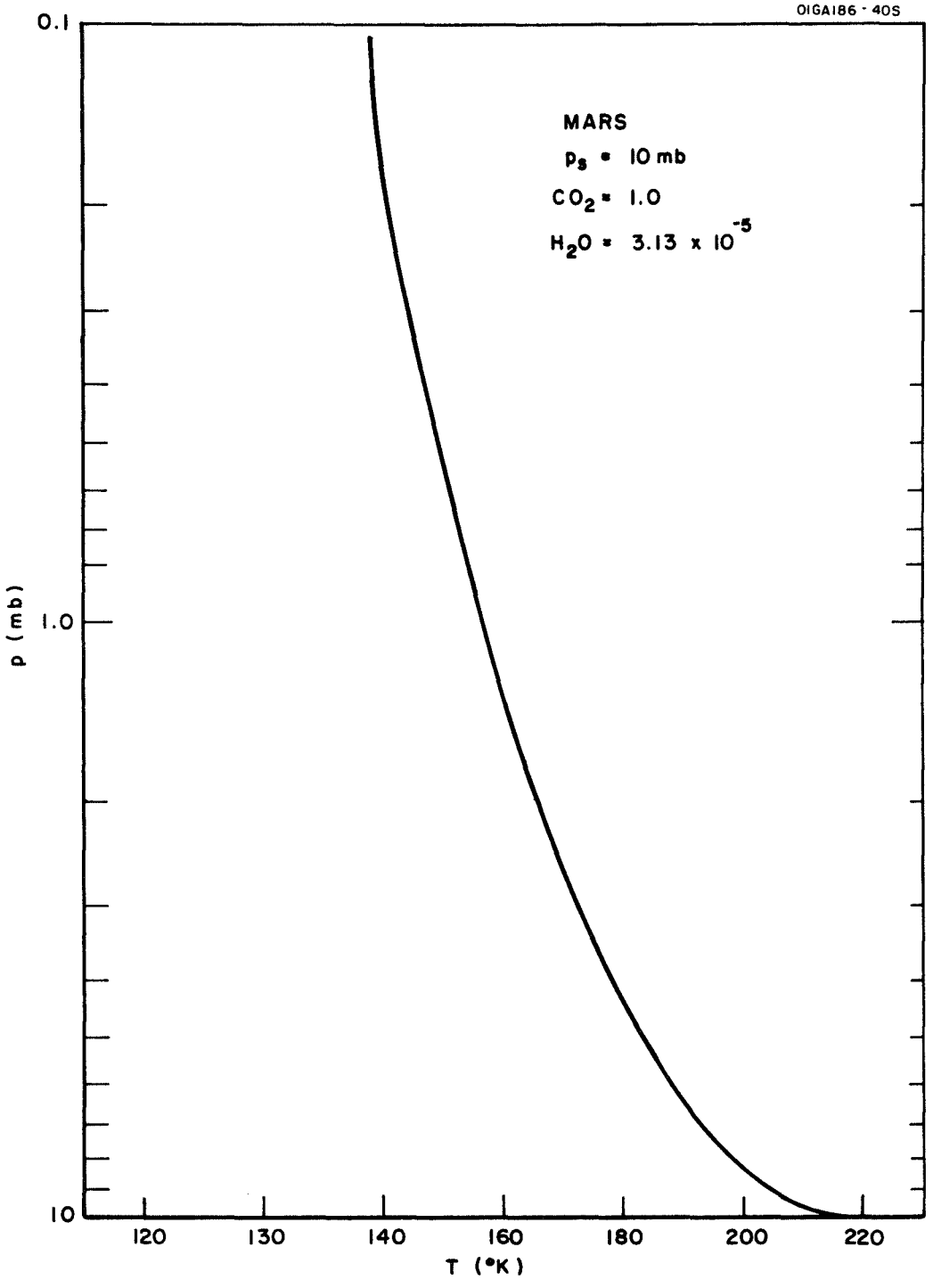

Figure 8. Mean radiative equilibrium temperature profile for Mars.

agreement between the computed radiative equilibrium profile and the mean observed temperature profile (standard atmosphere) for Earth must be considered good, in view of the fact that clouds, ozone, and the decrease of water vapor mixing ratio with altitude are not included in the model. The radiative equilibrium temperatures are lower than the actual temperatures in the stratosphere for two reasons: 1) the neglect of ozone, whose absorption of solar radiation heats the stratosphere, and 2) too high a water vapor mixing ratio in the stratosphere (3×10^{-3} versus an observed amount of $\sim 10^{-6}$), which increases the infrared cooling, and hence lowers the temperature of this region.

The calculation for Mars is in excellent agreement with previous radiative equilibrium (ref. 8) and radiative-convective equilibrium calculations (ref. 9) using the Rodgers and Walshaw (ref. 10) infrared transmittance model and the time marching method. The results for Earth and Mars lend confidence to the results for Venus and validate the iteration technique for optically thin atmospheres.

DISCUSSION AND CONCLUSIONS

Comparison of the radiative equilibrium temperature profile for the 65 atm model with the observed temperature profile for Venus suggests that the radiative processes included in the model control, to a large extent, the temperature structure of the Venusian atmosphere. However, there are a number of processes that have not been included in the present computations which would act to modify the computed profile. We shall attempt to discuss the qualitative effect of including these processes.

The computations of Samuelson (ref. 5) suggest that the inclusion of particulate clouds would increase the greenhouse effect over that for the purely gaseous absorbing atmosphere considered here. Thus, inclusion of particulate scattering and absorption processes would tend to increase the surface temperature.

The computed radiative equilibrium temperature lapse rate is unstable in the lower atmosphere. Convection would take place, transferring heat from surface to atmosphere, and causing a decrease in the surface temperature. Thus, inclusion of convective processes would tend to decrease the surface temperatures.

There are also a number of uncertainties concerning the input parameters. For example, the assumed water vapor mixing ratio of 10^{-5}, although within an order of magnitude of the generally low values obtained from Earth based spectroscopic observations (ref. 11) is 1/100 to 1/700 of that measured directly by Venera 4 (ref. 12). Any increase in the water vapor mixing ratio would increase the greenhouse effect, and, hence, the surface temperature. Also, an increase in water vapor mixing ratio would increase the infrared cooling of the upper atmosphere and tend to lower the radiative equilibrium temperatures in this region. The surface pressure may be even higher than 65 atm, perhaps more than 100 atm (ref. 13). Any increase in surface pressure would tend to increase the greenhouse effect, and hence, the radiative equilibrium surface temperature.

There is uncertainty concerning the validity of the infrared transmittance model at the high pressures and long carbon dioxide path lengths ($\sim 10^7$ atm-cm) of the Venus atmosphere. No one has measured infrared transmittances at these elevated pressures and path lengths. Thus, the extension of the strong line absorption law to higher pressures and path lengths, although founded in theory, has not been experimentally verified. In addition, collision-induced sources of infrared opacity are not included in the present infrared transmittance model. Inclusion of these collision-induced transitions would increase the greenhouse effect and surface temperature.

Despite the omission of potentially important processes and uncertainties in the input parameters, the good agreement between the computed radiative equilibrium temperature profile and the observed profile suggests that we have captured the essential physics of the thermal structure problem for Venus. To evaluate quantitatively some of the effects discussed above, we plan to incorporate such processes as convection, and scattering and absorption due to particulate matter and the cloud layer in future refinements of the model. In addition, we plan to compute the latitudinal and longitudinal variations of the temperature profile.

REFERENCES

1. Eshleman, V., G. Fjeldbo, J. Anderson, A. Kliore, and R. Dyce, 1968: Venus: Lower atmosphere not measured. Science, 162, 661-665.

2. Mintz, Y., 1961: Temperature and cir culation of the Venus atmosphere. Planet. Space Sci., 5, 141-152.

3. Bartko, F., and R. Hanel, 1968: Non-gray equilibrium temperature distributions above the clouds of Venus. Ap. J., 151, 365-378.

4. Jastrow, R., and S. Rasool, 1963: Radiative transfer in the atmospheres of Mars and Venus. In Space Research, v. 3, Wiley, New York, 1036-1041.

5. Samuelson, R.A., 1967: Greenhouse effect in semi-infinite scattering atmospheres: Application to Venus. Astrophys. J., 147, 782-798.

6. Manabe, S., and F. Moller, 1961: On the radiative equilibrium and heat balance of the atmosphere. Mon. Wea. Rev., 89, 503-532.

7. Jastrow, R., 1968: The planet Venus. Science, 160, 1403-1410.

8. Ohring, G., W. Tang, J. Mariano, and G. DeSanto, 1968a: Planetary meteorology. GCA Technical Report TR-68-4-N, 54 pp.

9. Ohring, G., and J. Mariano, 1968b: Seasonal and latitudinal variations of the average surface temperature and vertical temperature profile on Mars. J. Atmos. Sci., 25, 673-681.

10. Rodgers, C., and C. Walshaw, 1966: The computation of infrared cooling rates in planetary atmospheres. Quart. J. Roy. Met. Soc., 92, 67-92.

11. Belton, M., D. Hunten, and R. Goody, 1968: Quantitative spectroscopy of Venus in the region 8,000-11,000Å. In The Atmospheres of Mars and Venus, ed. J. Brandt and M. McElroy, Gordon and Breach, N. Y. 69-98.

12. Vinogradov, A., U. Surkov, and C. Florensky, 1968: The chemical composition of the Venus atmosphere based on the data of the interplanetary station Venera 4. J. Atmos. Sci., 25, 535-536.

13. Johnson, F., 1968: The atmosphere of Venus: A conference review. J. Atmos. Sci., 25, 658-662.

PART 3

INFRARED TRANSMITTANCE MODEL FOR PLANETARY ATMOSPHERES RESEARCH: EMPIRICAL FITS TO PLASS' CO_2 AND H_2O TRANSMITTANCE TABLES

George Ohring

INFRARED TRANSMITTANCE MODEL FOR PLANETARY ATMOSPHERES RESEARCH: EMPIRICAL FITS TO PLASS' CO_2 AND H_2O TRANSMITTANCE TABLES

ABSTRACT

Transmittance tables for carbon dioxide and water vapor, computed from a quasi-random band transmission model by Plass and co-workers, are fit, by least squares techniques, to a generalization of the strong line absorption law. The fits are for 100 cm^{-1} intervals, from 500 cm^{-1} to 10,000 cm^{-1} for CO_2, and from 1000 cm^{-1} for H_2O. For CO_2, the path length range covered is 10^3 to 2.37×10^7 atmo-cm, and the pressure range is 0.1 for 31 atm. For H_2O, the path length range covered is 10^{-3} to 50 precipitable cm, and the pressure range is 0.1 to 1 atm. For both CO_2 and H_2O, the temperature range is 200 to 300°K. Comparison of the empirical fits with the original data indicates that the path length and pressure dependence of the transmittance are being fit quite well, but that the temperature dependence could be improved upon. Overall root-mean-square difference between empirically fit and original transmittances is 0.10.

INTRODUCTION

In radiative calculations for planetary atmospheres, it is desirable to have a simple transmittance formula that is appropriate for the range of abosrber path lengths and pressures occurring in the particular planetary atmosphere. Many such models are available for the H_2O and CO_2 amounts, and surface pressures of the Earth's atmosphere. However, there are no available transmittance models that cover the range of CO_2 path lengths (of the order of 10^7 atmo-cm) and pressures (tens of atmospheres) found on Venus. The transmittance models of Bartko and Hanel (ref. 1), which we have used in our calculations for Venus, are based upon fitting a strong line absorption law to laboratory and calculated transmittance data. The laboratory and calculated transmittance data used for these fits do not include values comparable to those listed above. However, we can justify the extrapolated use of the Bartko/Hanel transmittance models because theoretically the strong line absorption law should also apply to the higher CO_2 amounts and surface pressures appropriate for Venus. To check on this; to develop an infrared transmittance model based upon calculated transmittances that include CO_2 path lengths and pressures applicable to Venus (ref. 2); and to provide the capability for rapidly computing transmittances of CO_2 and H_2O at 100 cm^{-1} resolution from 500 to 10,000 cm^{-1}, we have empirically fit the extensive CO_2 and H_2O transmittance tables computed by Plass and his co-workers. Although Venus is the immediate justification for this, the CO_2 and H_2O transmittance data assembled and punched on cards can also be processed, using techniques similar to that described below, for ranges of absorber path lengths and surface pressures applicable to other planets - Mars and Earth, for example.

FITTING PROCEDURE

Stull, et al. (ref. 3,4) and Plass and Stull (ref. 2) have calculated transmittances based on the quasi-random model of band absorption for the range of wave numbers, path lengths, pressures, and temperatures given in Table 1.

For application to Venus, we fit the following parts of Table 1. For CO_2, transmittance for path lengths greater than 10^3 atmo-cm and pressures greater than 0.1 atm. For H_2O, transmittance for pressures greater than 0.1 atm.

TABLE 1

RANGES COVERED BY PLASS TRANSMITTANCE TABLES

	Wavenumber Range(cm^{-1})	Path lengths	Pressures (atm)	Temperatures (^oK)
CO_2	600-10,000	0.2 to 10^4 atmo-cm	0.01 to 1	300, 250, 200
CO_2	500- 9,500	$10^5, 10^6, 2.37 \times 10^7$ atmo-cm	1, 10, 31	300
H_2O	1000-10,000	10^{-3} to 50 pr.cm	0.01 to 1	300, 250, 200

Based upon the strong line limit of the statistical band model of transmittance, Bartko and Hanel (ref. 1) derive the following transmission law for the case of appreciable overlapping of absorption lines

$$\tau_\nu = \exp\left[-\left(m_\nu u^*\right)^{n_\nu}\right] \qquad (1)$$

where

$$u^* = u\left(\frac{T_o}{T}\right)^{3/2} \exp\left[\gamma_\nu\left(\frac{1}{T_o} - \frac{1}{T}\right)\right]\left(\frac{p}{p_o}\right)^{k_\nu} \qquad (2)$$

and ν is wavenumber, τ is transmittance, u is path length of absorbing gas, T is temperature, p is pressure, the subscript o refers to standard conditions, $T_o = 273^oK$, $p_o = 1$ atm, and m_ν, n_ν, τ_ν, and k_ν are constants to be determined for each spectral interval. Bartko and Hanel assume that $n_\nu = k_\nu/2$. For the sake of generality, we shall not make such an assumption, letting n_ν and k_ν be derived from the fitting procedure.

To determine the coefficient of temperature dependence, we can take the natural log of $(1/\tau_{\nu 1})$, divide it by the natural log of $(1/\tau_{\nu 2})$, where $\tau_{\nu 1}$ and $\tau_{\nu 2}$ are transmittances for the same path length and pressure, but different temperatures, T_1 and T_2, to obtain

$$A_1 = \frac{\ell n\ (1/\tau_{\nu 1})}{\ell n\ (1/\tau_{\nu 2})} = \left[\frac{\exp(-\gamma_\nu/T_1)}{\exp(-\gamma_\nu/T_2)} \left(\frac{T_2}{T_1}\right)^{3/2} \right]^{n_\nu} \tag{3}$$

By defining a similar ratio for another pair of temperatures, T_2 and T_3, taking natural logs, and dividing, we obtain

$$\frac{\ell n\ A_1}{\ell n\ A_2} = \frac{\gamma_\nu \left(\frac{1}{T_2} - \frac{1}{T_1}\right) + 1.5\ \ell n(T_2/T_1)}{\gamma_\nu \left(\frac{1}{T_3} - \frac{1}{T_2}\right) + 1.5\ \ell n(T_3/T_2)} \tag{4}$$

Solving for γ, we obtain

$$\gamma_\nu = \frac{C_1\ \ell n\ A_2 - C_2\ \ell n\ A_1}{B_2\ \ell n\ A_1 - B_1\ \ell n\ A_2} \tag{5}$$

where B_1, B_2, C_1, and C_2 are constants that depend upon the temperatures used as follows.

$$B_1 = \frac{1}{T_2} - \frac{1}{T_1} \tag{6}$$

$$B_2 = \frac{1}{T_3} - \frac{1}{T_2} \tag{7}$$

$$C_1 = 1.5\ \ell n(T_2/T_1) \tag{8}$$

$$C_2 = 1.5\ \ell n(T_3/T_2) \tag{9}$$

In the Plass tables, transmittances are tabulated for three temperatures: $T_1 = 300^{\circ}K$, $T_2 = 250^{\circ}K$, and $T_3 = 200^{\circ}K$. Two different methods were used to determine the average value of γ for a spectral interval. In the first method, the average values of $\ell n\ A_1$ and $\ell n\ A_2$ are computed from sets of transmittance data, each set consisting of a value of transmittance at each of the three temperatures, and γ is found from

$$\overline{\gamma_\nu} = \frac{C_1\ \overline{\ell n\ A_2} - C_2\ \overline{\ell n\ A_1}}{B_2\ \overline{\ell n\ A_1} - B_1\ \overline{\ell n\ A_2}} \tag{10}$$

In the second method, the average value of γ is determined from a simple average of individual values of γ computed for each set of three transmittances at different temperatures but similar path lengths and pressures. In this case,

$$\overline{\gamma_\nu} = \sum_{i=1}^{N} \frac{\gamma_{\nu_i}}{N} \tag{11}$$

where γ_ν is computed from Equation (5) and N is the number of sets of transmittances.

In both methods, all transmittances equal to 0 or 1 are not used in the computations. The transmittance data for the ranges indicated by rows 1 and 3 of Table 2 are used to derive values of $\overline{\gamma}$ for each 100 cm^{-1} spectral interval.

TABLE 2

RANGES OF PARAMETERS IN FITTING PROCEDURE

	Wavenumber Range(cm^{-1})	Path lengths	Pressures (atm)	Temperatures (^oK)
CO_2	600- 9,500	10^3 to 10^4 atmo-cm	0.1 to 1	300,250,200
CO_2	600- 9,500	10^5, 10^6, 2.37×10^7 atmo-cm	1, 10, 31	300
H_2O	1000-10,000	10^{-3} to 50 pr. cm	0.1 to 1	300,250,200

Once the temperature coefficient γ is found, the other constants, m_ν, k_ν, and n_ν, can be determined from a least squares fitting procedure, as follows.

Substitution of Equation (2) into Equation (1) leads to

$$\tau_\nu = \exp - \left[c_\nu T^{-1.5} \exp\left(-\frac{\gamma_\nu}{T}\right) u\, p^{k_\nu} \right]^{n_\nu} \qquad (12)$$

where

$$c_\nu = T_o^{1.5}\, p_o^{-k_\nu} \exp\left(\frac{\gamma_\nu}{T_o}\right) m_\nu \qquad (13)$$

Taking ℓn (ℓn $1/\tau_\nu$), we obtain

$$\ell n \left(\ell n \frac{1}{\tau_\nu}\right) = n_\nu \ \ell n\, c_\nu + n_\nu \ell n \left[T^{-1.5} \exp\left(-\frac{\gamma_\nu}{T}\right)\right] + n_\nu \ \ell n\, u + n_\nu k_\nu \ \ell n\, p \qquad (14)$$

Letting

$$a_\nu = n_\nu \ \ell n \ c_\nu \tag{15}$$

$$F = \ell n \left[T^{-1.5} \exp \left(- \frac{\gamma_\nu}{T} \right) \right] \tag{16}$$

$$U = \ell n \ u \tag{17}$$

$$P = \ell n \ p \tag{18}$$

$$b_\nu = n_\nu \ k_\nu \tag{19}$$

and

$$W_\nu = \ell n \left(\ell n \ \frac{1}{\tau_\nu} \right) \tag{20}$$

we can rewrite Equation (14) as

$$W_\nu = a_\nu + n_\nu (F + U) + b_\nu \ P \tag{21}$$

or

$$W_\nu = a_\nu + n_\nu \ G + b_\nu \ P \tag{22}$$

where

$$G = F + U \tag{23}$$

The constants a_ν, n_ν, and b_ν, and, from them, the constants m_ν, k_ν, and n_ν, can be determined from a least squares fit of Equation (22) to the transmittance data.

For both CO_2 and H_2O, the transmittance data for a temperature of 300°K, and for the path length and pressure ranges indicated in Table 2, are used in the least squares fit. Any transmittances equal to 0 or 1 are not used in the fitting procedure.

To evaluate the goodness of fit, three types of statistics are

computed: The mean of the absolute values of the relative errors, the mean deviation, and the root-mean-square error. These are defined as follows. Mean of absolute values of relative errors =

$$\overline{|R.E.|} = \frac{\sum_{i=1}^{N} \left(|\tau_c - \tau_o| \Big/ \tau_{oi} \right)}{N} \tag{24}$$

where the τ_c are the transmittances computed from Equation (22) and the τ_o are the original transmittances in the Plass tables. N is the number of pairs of transmittances.

Mean deviation =

$$\overline{D} = \frac{\sum_{i=1}^{N} (\tau_c - \tau_o)_i}{N} \tag{25}$$

Root-mean-square error =

$$RMS = \left\{ \frac{\sum_{i=1}^{N} (\tau_c - \tau_o)_i^2}{N} \right\}^{1/2} \tag{26}$$

RESULTS

The derived constants for each spectral interval for both water vapor and carbon dioxide are shown in Table 3. Dashes indicate insufficient transmittance data to determine constants. All constants have been rounded off to two significant digits. The two methods for computing γ are indicated by γ-pack. 1 and γ-pack. 2.

It can be seen that significantly different values of γ may result, depending upon which method is used for its determination. Also, in some instances γ is computed to be negative, which is theoretically forbidden. This is due to the extreme sensitivity of both methods of computing γ to the transmittance values, which are only tabulated to three decimal places in the Plass tables.

Error statistics were computed for all wavelength intervals, for each of the three temperatures. Tables 4 to 7 are samples of the computed error statistics; complete tables of the error statistics may be found in Ohring (ref. 5).

TABLE 3

EMPIRICAL CONSTANTS FOR H_2O AND CO_2 INFRARED TRANSMITTANCE

	H_2O						CO_2					
			γ-Pack. 1		γ-Pack. 2				γ-Pack. 1		γ-Pack. 2	
ν (cm^{-1})	k	n	m (pr. cm)$^{-1}$	γ	m (pr. cm)$^{-1}$	γ	k	n	m (atmo-cm)$^{-1}$	γ	m (atmo-cm)$^{-1}$	γ
650							1.0	0.35	8.7E-1	- 370	7.3E-1	160
750							0.80	0.34	4.9E-3	190	4.9E-3	170
850							0.72	0.62	1.9E-4	- 70	1.5E-4	730
950							0.56	0.68	9.8E-5	-3800	2.8E-5	- 50
1050	0.49	0.95	1.5E-2	290	1.4E-2	410	0.74	0.52	3.7E-5	1500	8.1E-5	- 850
1150	0.43	0.76	4.0E-2	- 210	3.6E-2	250	0.53	0.94	8.2E-7	330	8.2E-7	330
1250	0.44	0.71	2.2E-1	230	2.0E-1	500	1.0	1.0	1.1E-7	—	1.1E-7	—
1350	0.75	0.52	3.7	- 180	2.8	690	1.1	1.1	5.4E-8	—	5.4E-8	—
1450	0.86	0.54	3.1E+1	400	3.1E+1	400	1.0	1.0	6.9E-8	—	6.9E-8	—
1550	0.90	0.46	5.6E+1	- 100	5.3E+1	70	1.1	0.99	1.4E-7	—	1.4E-7	—
1650	0.93	0.48	7.6E+1	- 90	7.2E+1	50	1.0	0.96	3.4E-7	—	3.4E-7	—
1750	0.91	0.52	6.3E+1	100	6.4E+1	50	1.0	0.91	9.4E-7	—	9.4E-7	—
1850	0.86	0.55	1.9E+1	- 590	1.5E+1	170	0.48	0.90	5.8E-6	230	6.0E-6	130
1950	0.84	0.54	3.0	840	2.9	960	0.60	0.62	4.5E-5	220	4.5E-5	220
2050	0.72	0.59	3.0E+2	-18000	8.1E-1	420	0.69	0.53	2.6E-4	240	2.6E-4	240
2150	0.47	0.69	2.3E-1	- 160	2.1E-1	120	0.87	0.83	4.9E-4	240	4.9E-4	250
2250	0.43	0.74	4.9E-2	- 40	3.5E-2	960	0.85	0.38	2.2E-2	290	2.2E-2	290
2350	0.47	0.80	1.3E-2	300	1.6E-2	-460	—	—	—	—	—	—
2450	0.68	0.86	9.6E-3	340	9.5E-3	380	1.0	0.65	3.4E-3	- 100	3.1E-3	240
2550	0.54	1.0	1.2E-2	350	1.1E-2	460	0.99	0.98	2.8E-4	0	2.9E-4	- 40
2650	0.39	0.87	1.7E-2	250	1.9E-2	- 80	0.93	1.4	9.1E-5	10	9.3E-5	0
2750	0.32	0.78	3.1E-2	690	4.2E-2	-180	1.3	1.0	7.2E-6	10	7.3E-6	40
2850	0.36	0.81	3.4E-2	1400	4.7E-2	330	0.95	1.1	2.5E-6	- 180	2.8E-6	- 520
2950	0.59	0.64	1.6E-1	540	1.7E-1	390	0.90	1.4	8.3E-7	- 230	8.3E-7	- 230
3050	0.65	0.58	6.0E-1	140	6.0E-1	150	1.0	0.99	3.4E-7	—	3.4E-7	—
3150	0.65	0.57	9.4E-1	- 170	8.3E-1	220	1.0	1.0	2.3E-7	—	2.3E-7	—
3250	0.70	0.58	1.8	- 170	1.3	920	1.0	0.94	3.7E-7	—	3.7E-7	—
3350	0.73	0.61	1.7	460	1.7	470	0.45	0.75	5.5E-6	80	5.9E-6	- 90

TABLE 3 (continued)

	H_2O						CO_2					
			γ-Pack. 1		γ-Pack. 2				γ-Pack. 1		γ-Pack. 2	
ν_1 (cm^{-1})	k	n	m $(pr.\ cm)^{-1}$	γ	m $(pr.\ cm)^{-1}$	γ	k	n	m $(atmo\text{-}cm)^{-1}$	γ	m $(atmo\text{-}cm)^{-1}$	γ
3450	0.80	0.57	5.1	700	9.2	-1100	0.61	0.53	1.6E-4	110	1.6E-4	90
3550	0.84	0.54	3.2E+1	310	3.2E+1	300	0.76	0.43	1.8E-2	250	1.8E-2	250
3650	0.85	0.55	7.5E+1	450	7.5E+1	450	0.99	0.46	1.5E-1	170	1.5E-1	130
3750	0.86	0.44	1.5E+2	330	1.5E+2	310	0.92	0.31	3.3E-3	270	3.3E-3	260
3850	0.91	0.54	9.2E+1	530	9.3E+1	510	0.74	0.64	5.9E-5	80	7.3E-5	- 570
3950	0.88	0.51	1.4E+1	580	1.6E+1	320	0.91	1.1	2.4E-6	- 630	1.1E-7	8700
4050	0.66	0.62	2.4E-1	2500	5.4E-1	84	1.0	0.88	4.6E-7	—	4.6E-7	—
4150	0.68	1.1	8.9E-2	390	8.6E-2	480	1.0	0.95	1.2E-7	—	1.2E-7	—
4250	0.84	1.3	5.7E-2	620	1.7E-1	-2700	1.1	1.1	3.4E-8	—	3.4E-8	—
4350	0.86	1.2	4.1E-2	520	3.2E-2	1240	1.2	1.3	1.1E-8	—	1.1E-8	—
4450	0.63	0.78	3.2E-2	320	2.9E-2	650	0.63	1.3	2.3E-8	—	2.3E-8	—
4550	0.59	0.67	6.5E-2	260	6.7E-2	160	0.43	1.3	5.5E-8	—	5.5E-8	—
4650	0.44	0.65	9.3E-2	180	8.7E-2	370	0.22	0.82	9.2E-7	- 10	7.8E-7	500
4750	0.49	0.64	5.1E-2	450	5.3E-2	360	0.58	0.51	2.9E-5	190	2.9E-5	190
4850	0.50	0.66	7.7E-2	160	9.0E-2	- 350	0.81	0.57	9.1E-4	- 220	2.0E-4	4300
4950	0.55	0.68	1.4E-1	- 1000	9.7E-2	130	0.74	0.47	1.2E-3	200	1.2E-3	200
5050	0.50	0.66	3.1E-1	- 170	2.7E-1	240	0.73	0.54	2.1E-4	190	2.1E-4	190
5150	0.72	0.57	5.0	- 2000	1.9	900	0.83	0.32	2.5E-5	130	2.5E-5	120
5250	0.83	0.56	8.1	100	8.2	70	0.25	0.91	9.1E-7	110	9.5E-7	- 20
5350	0.84	0.48	2.2E+1	- 350	1.8E+1	280	1.1	1.1	5.9E-9	—	5.9E-9	—
5450	0.86	0.54	5.4	420	5.4	420	0.37	1.4	2.5E-8	—	2.5E-8	—
5550	0.76	0.55	1.1	500	1.1	500	0.23	0.88	1.3E-7	—	1.3E-7	—
5650	0.38	0.69	1.4E-1	- 470	3.8E-1	-3600	0.18	0.83	1.7E-7	—	1.7E-7	—
5750	0.39	0.75	3.2E-2	130	1.1E-2	3300	0.32	0.67	6.1E-9	—	6.1E-9	—
5850	0.32	0.86	1.2E-2	250	1.1E-2	370	0.15	1.0	9.4E-9	—	9.4E-9	—
5950	0.35	0.76	9.9E-3	190	8.4E-3	390	0.18	0.91	1.7E-7	330	1.7E-7	330
6050	0.48	0.71	1.5E-2	370	1.6E-2	320	0.32	0.73	2.2E-6	230	2.1E-6	350
6150	0.31	0.71	2.4E-2	410	2.4E-2	410	0.29	0.75	4.4E-6	10	4.8E-6	- 290
6250	0.31	0.73	2.6E-2	580	2.8E-2	410	0.58	0.50	6.0E-6	330	6.0E-6	310

TABLE 3 (continued)

	H_2O						CO_2					
			γ-Pack. 1		γ-Pack. 2				γ-Pack. 1		γ-Pack. 2	
ν (cm^{-1})	k	n	m $(pr.\ cm)^{-1}$	γ	m $(pr.\ cm)^{-1}$	γ	k	n	m $(atmo\text{-}cm)^{-1}$	γ	m $(atmo\text{-}cm)^{-1}$	γ
6350	0.26	0.78	6.1E-2	300	6.1E-2	300	0.66	0.45	5.9E-6	210	5.9E-6	210
6450	0.26	0.80	9.1E-2	300	9.3E-2	230	0.39	0.67	7.4E-7	310	7.2E-7	360
6550	0.30	0.78	8.1E-2	320	8.2E-2	260	0.35	0.58	4.0E-7	290	4.9E-7	310
6650	0.37	0.71	9.0E-2	180	8.7E-2	260	0.21	1.0	4.6E-8	—	4.6E-8	—
6750	0.49	0.66	3.2E-1	70	2.7E-1	540	0.27	0.74	1.7E-6	320	1.7E-6	290
6850	0.56	0.60	4.1E-1	770	3.8E-1	970	0.23	0.73	1.6E-6	160	1.6E-6	200
6950	0.56	0.63	8.3E-1	- 430	4.8E-1	1200	0.86	0.46	8.2E-5	- 300	5.4E-5	1000
7050	0.63	0.61	1.9	410	1.9	410	0.44	0.87	3.5E-7	270	3.3E-7	450
7150	0.69	0.58	3.9	350	3.9	350	0.19	0.95	1.8E-7	330	1.8E-7	330
7250	0.77	0.50	6.6	200	6.6	220	0.22	0.78	1.3E-6	370	1.3E-6	370
7350	0.74	0.57	5.2	480	6.3	- 90	0.23	0.83	3.3E-6	250	3.3E-6	200
7450	0.63	0.61	2.4	430	2.4	470	0.58	0.57	1.9E-5	210	2.0E-5	180
7550	0.69	0.59	6.0E-1	450	6.0E-1	460	0.58	0.46	9.9E-6	260	1.0E-5	230
7650	0.67	0.60	3.5E-1	350	3.5E-1	350	0.67	0.45	4.6E-6	210	4.6E-6	190
7750	0.40	0.71	3.9E-2	200	4.1E-2	120	0.59	0.46	5.7E-6	240	5.7E-6	250
7850	0.28	0.82	4.6E-3	160	4.1E-3	470	0.23	0.81	3.3E-7	170	3.4E-7	130
7950	0.30	0.75	1.2E-3	350	1.2E-3	360	0.29	0.67	7.2E-7	- 500	5.4E-7	360
8050	0.35	0.74	3.9E-3	530	4.0E-3	460	0.18	1.1	2.6E-8	—	2.6E-8	—
8150	0.32	0.74	1.1E-2	350	1.1E-2	350	0.17	0.85	1.4E-7	—	1.4E-7	—
8250	0.37	0.73	5.0E-2	270	5.0E-2	280	0.13	0.79	1.6E-7	—	1.6E-7	—
8350	0.39	0.65	6.4E-2	260	6.5E-2	220	0.32	0.65	1.3E-8	410	1.3E-8	410
8450	0.46	0.67	6.1E-2	310	6.1E-2	310	0	1.2	4.1E-9	—	4.1E-9	—
8550	0.36	0.72	4.5E-2	410	4.5E-2	410	0	1.1	5.0E-9	—	5.0E-9	—
8650	0.41	0.70	8.0E-2	440	8.0E-2	420	0.16	0.93	2.9E-8	—	2.9E-8	—
8750	0.41	0.69	1.4E-1	410	1.4E-1	390	0.17	0.92	2.4E-8	—	2.4E-8	—
8850	0.47	0.62	1.8E-1	440	1.8E-1	440	0.19	0.77	9.8E-8	330	9.8E-8	330
8950	0.40	0.69	1.3E-1	320	1.3E-1	310	0.15	0.77	1.2E-7	330	1.2E-7	330
9050	0.31	0.75	4.7E-2	470	2.5E-2	2400	0.32	1.0	3.8E-9	—	3.8E-9	—
9150	0.43	0.69	2.1E-2	- 320	1.3E-2	1000	0.09	0.84	3.4E-8	—	3.4E-8	—

TABLE 3 (continued)

	H_2O						CO_2					
			γ-Pack. 1		γ-Pack. 2				γ-Pack. 1		γ-Pack. 2	
ν (cm^{-1})	k	n	m $(pr.\ cm)^{-1}$	γ	m $(pr.\ cm)^{-1}$	γ	k	n	m $(atmo\text{-}cm)^{-1}$	γ	m $(atmo\text{-}cm)^{-1}$	γ
9250	0.39	0.73	1.0E-2	340	9.9E-3	360	0.14	0.71	1.7E-10	——	1.7E-10	——
9350	0.34	0.75	2.4E-3	160	2.3E-3	230	0.14	1.1	1.2E-8	——	1.2E-8	——
9450	0.19	0.79	4.7E-4	70	3.8E-4	700	0.11	1.1	1.4E-8	——	1.4E-8	——
9550	0.20	0.89	1.3E-3	790	1.4E-3	540						
9650	0.33	0.78	4.9E-3	330	4.9E-3	330						
9750	0.35	0.73	8.3E-3	190	8.4E-3	150						
9850	0.36	0.68	1.6E-2	- 720	1.2E-2	270						
9950	0.33	0.75	1.5E-2	250	1.5E-2	390						

TABLE 4

SAMPLE OF ERROR STATISTICS FOR CO_2(γ-PACK. 1) TRANSMITTANCE FITS

For each wavenumber, first row is $\overline{|R.E.|}$, second row is D, third row is RMS, and fourth row is number of pairs of transmittances

Wavenumber (cm^{-1})	T = 300°K	T = 250°K	T = 200°K
650	0.046	0.889	0.996
	-0.000	-0.009	-0.019
	0.000	0.013	0.029
	4.000	6.000	10.000
750	0.084	0.400	0.599
	-0.001	-0.096	-0.196
	0.011	0.100	0.205
	16.000	16.000	16.000
850	0.017	0.298	0.451
	-0.000	-0.225	-0.397
	0.010	0.236	0.417
	16.000	16.000	16.000
950	0.006	0.530	0.998
	0.001	-0.492	-0.980
	0.007	0.524	0.980
	16.000	16.000	16.000
1050	0.058	0.058	0.063
	0.006	-0.049	-0.060
	0.016	0.051	0.066
	17.000	16.000	16.000
1150	0.602	0.006	0.010
	0.005	-0.006	-0.010
	0.073	0.006	0.010
	20.000	4.000	1.000

TABLE 5

SAMPLE OF ERROR STATISTICS FOR CO_2 (γ-PACK. 2) TRANSMITTANCE FITS

For each wavenumber, first row is $\overline{|R.E.|}$, second row is D, third row is RMS, and fourth row is number of pairs of transmittances

Wavenumber (cm^{-1})	T = 300°K	T = 250°K	T = 200°K
650	0.046	0.745	0.965
	-0.000	-0.008	-0.018
	0.000	0.011	0.026
	4.000	6.000	10.000
750	0.084	0.404	0.605
	-0.001	-0.096	-0.198
	0.011	0.101	0.207
	16.000	16.000	16.000
850	0.017	0.184	0.209
	-0.000	-0.139	-0.183
	0.010	0.146	0.194
	16.000	16.000	16.000
950	0.006	0.105	0.178
	0.001	-0.097	-0.173
	0.007	0.110	0.198
	16.000	16.000	16.000
1050	0.058	0.263	0.513
	0.006	-0.221	-0.489
	0.016	0.234	0.514
	17.000	16.000	16.000
1150	0.602	0.006	0.010
	0.005	-0.006	-0.010
	0.073	0.006	0.010
	20.000	4.000	1.000

TABLE 6

SAMPLE OF ERROR STATISTICS FOR H_2O (γ-PACK. 1) TRANSMITTANCE FITS

For each wavenumber, first row is $\overline{|R.E.|}$, second row is D, third row is RMS, and fourth row is number of pairs of transmittances

Wavenumber (cm^{-1})	T = 300°K	T = 250°K	T = 200°K
1050	0.049	0.079	0.189
	0.007	0.004	0.028
	0.050	0.063	0.098
	20.000	16.000	14.000
1150	0.080	0.095	0.167
	0.000	-0.040	-0.090
	0.049	0.080	0.134
	28.000	24.000	20.000
1250	0.100	0.132	0.194
	-0.004	-0.041	-0.077
	0.049	0.078	0.118
	32.000	32.000	28.000
1350	0.151	0.295	0.441
	0.015	-0.047	-0.124
	0.030	0.055	0.150
	30.000	31.000	31.000
1450	0.073	0.066	0.074
	0.000	0.000	0.004
	0.006	0.006	0.009
	24.000	24.000	24.000
1550	0.097	0.104	0.134
	0.007	-0.006	-0.026
	0.018	0.012	0.030
	24.000	24.000	22.000

TABLE 7

SAMPLE OF ERROR STATISTICS FOR H_2O (γ-PACK. 2) TRANSMITTANCE FITS

For each wavenumber, first row is $\overline{|R.E.|}$, second row is D, third row is RMS, and fourth row is number of pairs of transmittances

Wavenumber (cm^{-1})	T = 300°K	T = 250°K	T = 200°K
1050	0.049	0.085	0.229
	0.007	0.012	0.049
	0.050	0.068	0.120
	20.000	16.000	14.000
1150	0.080	0.100	0.202
	0.000	-0.023	-0.037
	0.049	0.066	0.086
	28.000	24.000	20.000
1250	0.100	0.106	0.205
	-0.004	-0.026	-0.036
	0.049	0.062	0.072
	32.000	32.000	28.000
1350	0.151	0.147	0.094
	0.015	0.001	-0.005
	0.030	0.018	0.016
	31.000	31.000	31.000
1450	0.073	0.066	0.073
	0.000	0.000	0.004
	0.006	0.006	0.009
	24.000	24.000	24.000
1550	0.097	0.072	0.117
	0.007	0.005	0.003
	0.018	0.015	0.014
	24.000	24.000	22.000

In general, the fit is quite good for all spectral intervals at $T = 300^{\circ}K$. The errors increase at $T = 250^{\circ}K$ and $T = 200^{\circ}K$, suggesting that the temperature dependence could be improved upon. Some of the large mean relative errors are due to one or two large relative errors at low transmittance values. For example, an original τ of approximately 0.001 and computed τ of approximately 0.005 would yield a relative error of 4, which, if part of a small sample, would lead to a large mean relative error. The overall RMS errors for both CO_2 and H_2O are approximately 0.10. This can be significantly improved upon if one uses for each spectral interval the value of γ yielding the lowest RMS error.

Figures 1 through 4 illustrate some comparisons between the computed and the original transmittances for carbon dioxide. Figure 1 illustrates for sample wavelengths centered at 1850 cm^{-1} and 1050 cm^{-1} how well the path length dependence of transmittance is being accounted for. Figure 2 shows a comparison of the original and computed pressure dependence of transmittance at high pressures for a sample wavelength of 1250 cm^{-1}. Figure 3 also compares the pressure dependence, but for the lower values of pressure. Figure 4 illustrates original and computed transmittances at ν = 1050 cm^{-1} for different temperatures. These sample graphs illustrate what has already been shown by the error statistics - namely, that the major dependence of transmittance upon path length and pressure is being accounted for quite well by the empirical transmittance formulas while the dependence of transmittance upon temperature is not being accounted for as well.

Comparison of the present results with the empirical constants of Bartko and Hanel (ref. 1) is difficult because only one of their spectral intervals is 100 cm^{-1} wide. However, to obtain a rough indication of what such a comparison might show, we have averaged their constants for regions of the spectrum in which their spectral resolution is better than 100 cm^{-1}, and have averaged our constants for regions of the spectrum in which their results are for spectral resolution poorer than 100 cm^{-1}. Simple weighted (according to spectral width) averages of the constants may not be appropriate since some of the constants (m, for example) may vary quite rapidly with wavenumber. The comparison of the Bartko and Hanel constants (B&H) and the present constants (0), derived as indicated above, is shown in Table 8. The one spectral interval in which no averaging had to be performed, 1000 - 1100 cm^{-1}, shows the smallest differences between the two sets of results. In general, values of m, k, and n compare fairly well with each other. The present values of γ for CO_2 are consistently lower than the Bartko and Hanel values.

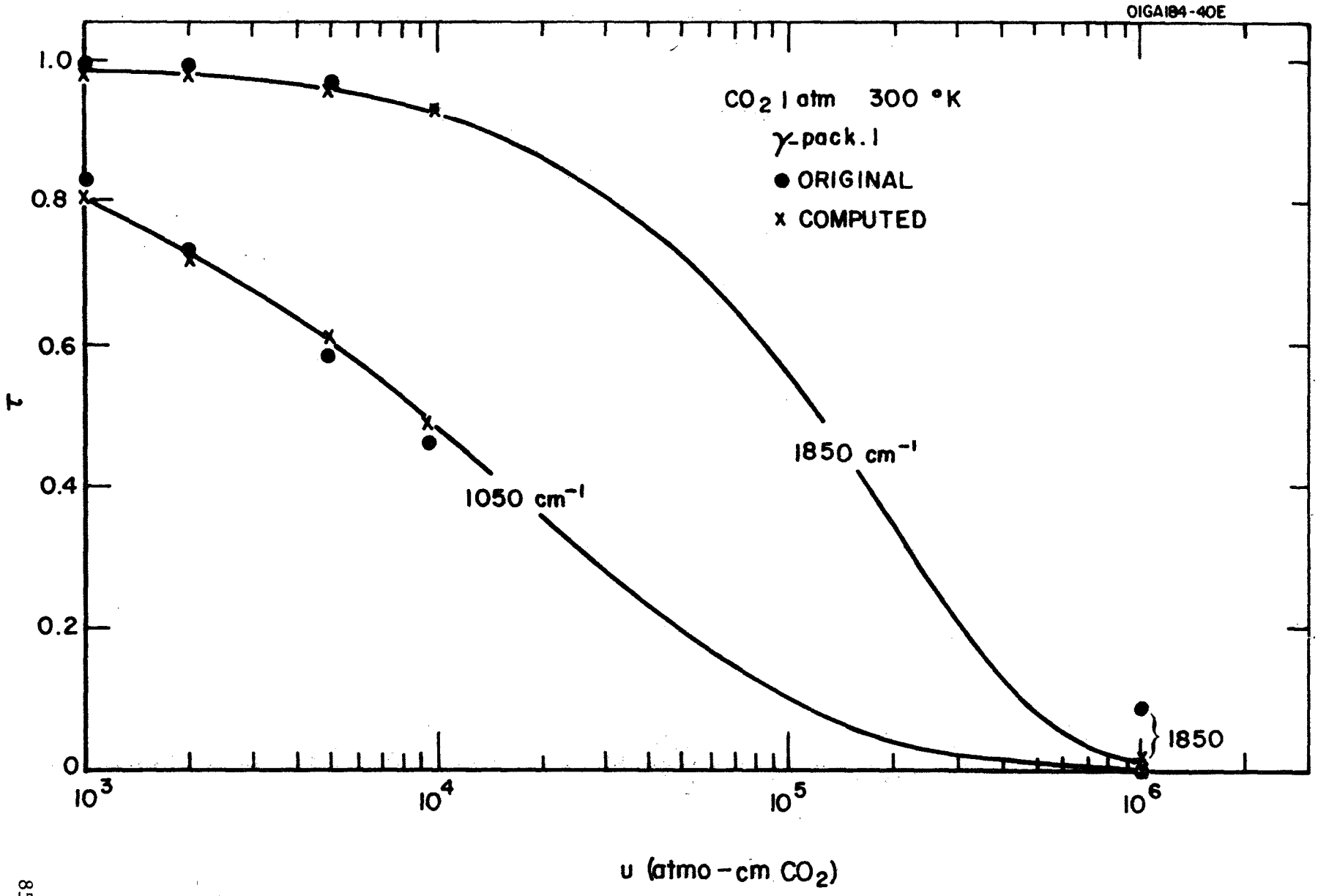

Figure 1. Original and computed CO_2 transmittances at 1850 cm^{-1} and 1050 cm^{-1} versus pathlength.

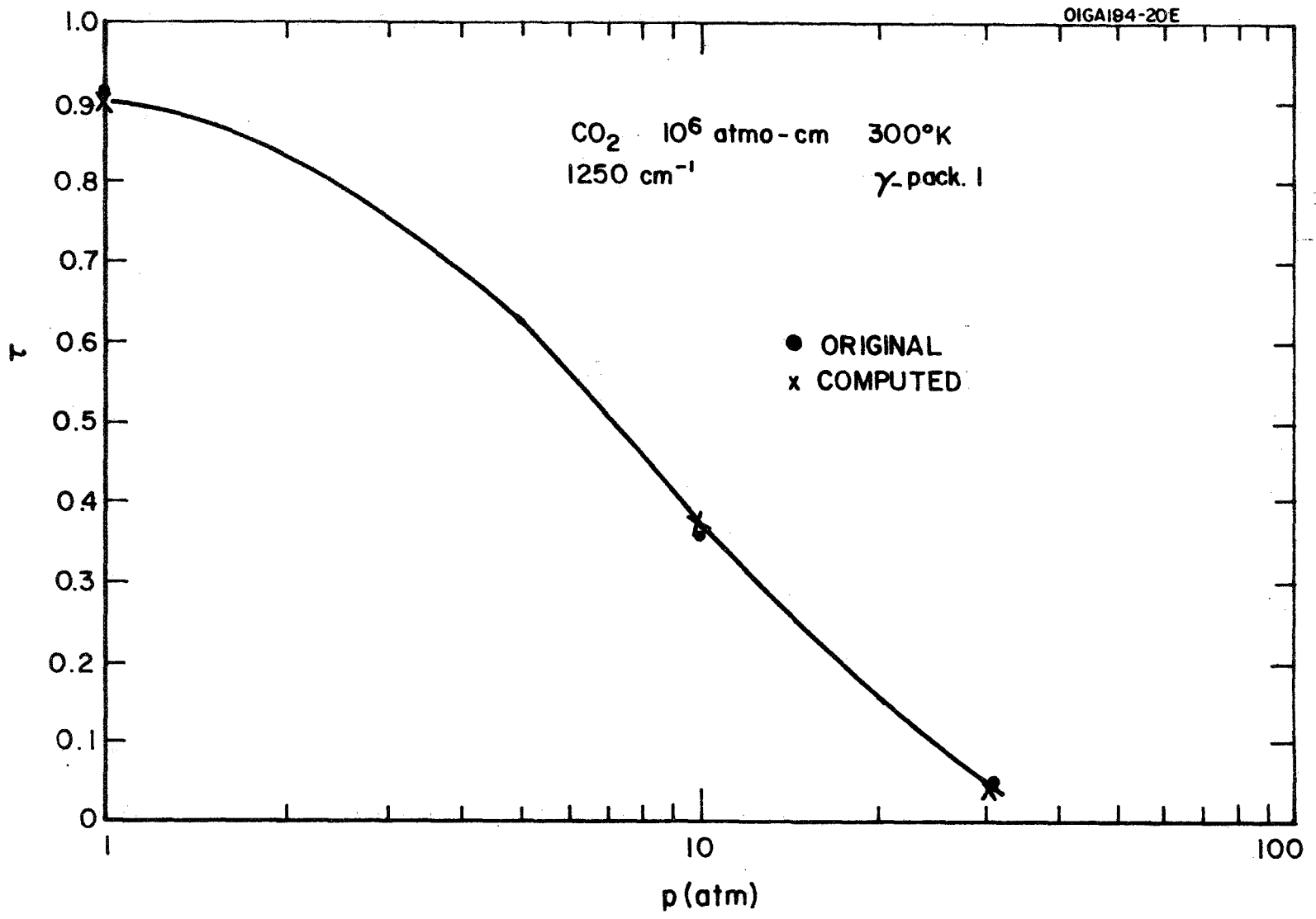

Figure 2. Original and computed CO_2 transmittances at 1250 cm^{-1} versus pressure.

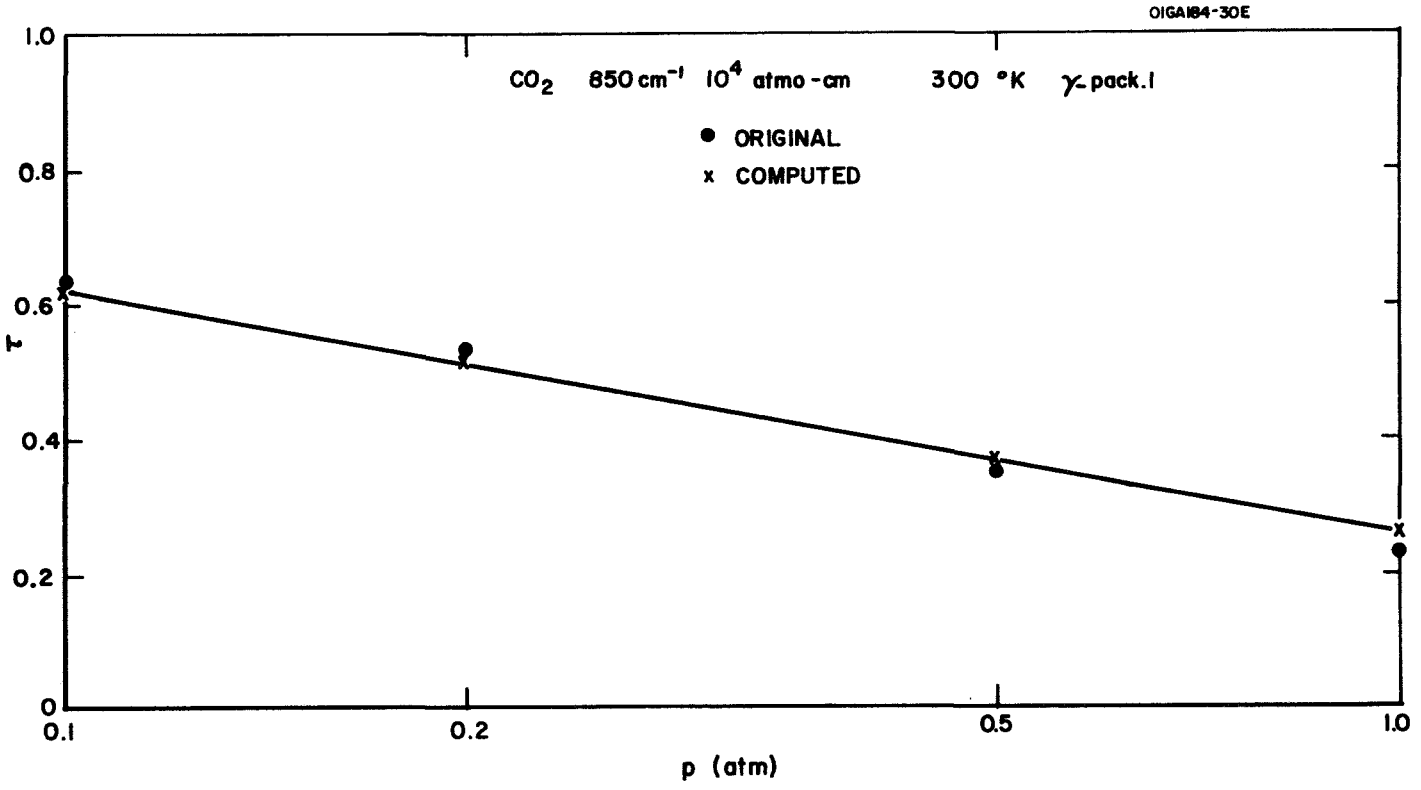

Figure 3. Original and computed CO_2 transmittances at 850 cm^{-1} versus pressure.

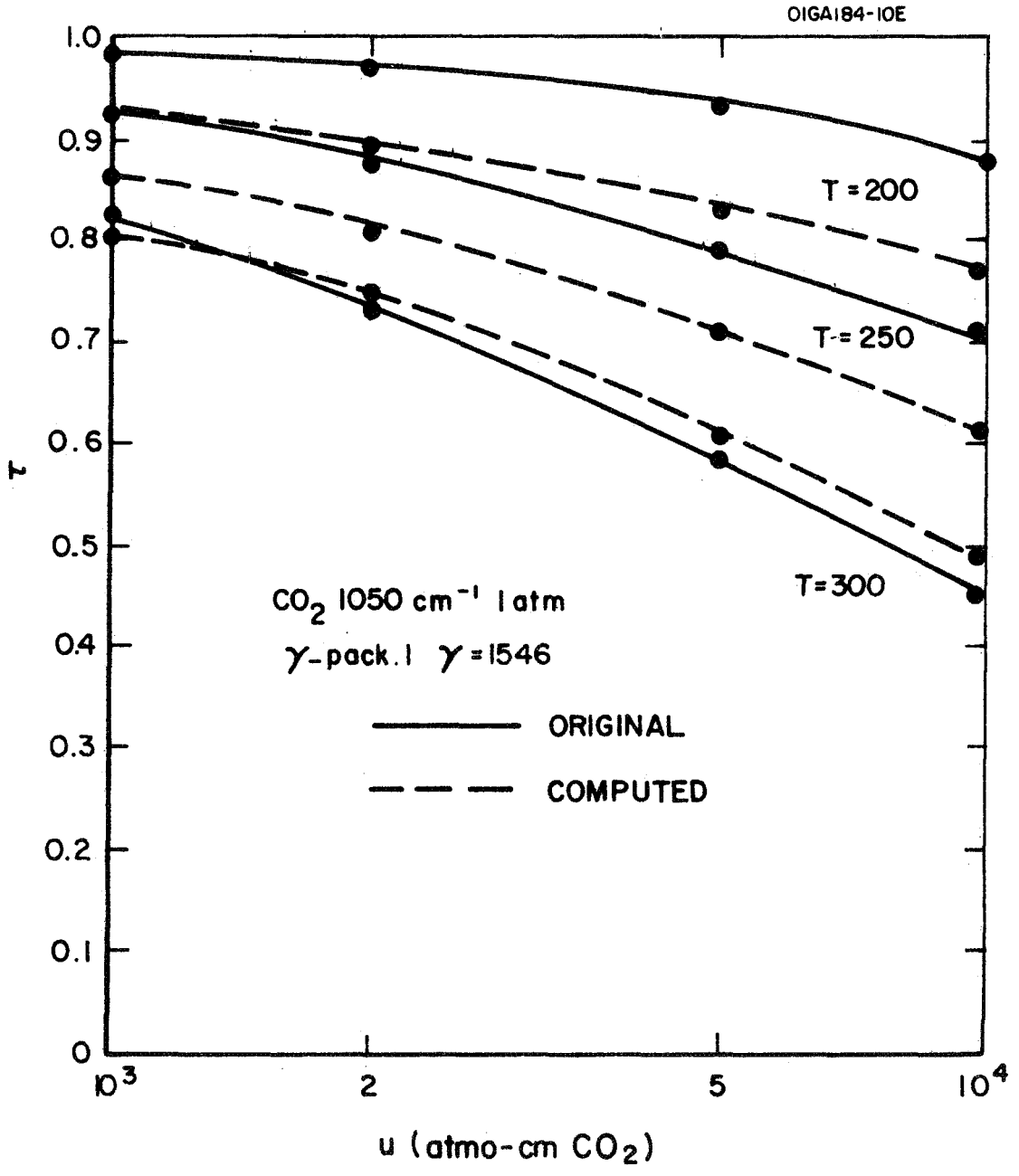

Figure 4. Original and computed CO_2 transmittances at 1050 cm^{-1} versus pathlength for three different temperatures.

TABLE 8

ROUGH COMPARISON OF EMPIRICAL CONSTANTS DERIVED BY BARTKO AND HANEL (ref. 1) WITH THOSE DERIVED IN PRESENT STUDY(O)

$\nu(cm^{-1})$	m		n		k		γ	
	B&H	O	B&H	O	B&H	O	B&H	O
			CO_2					
600- 700	4.6×10^{-1}	7.3×10^{-1}	0.39	0.35	0.78	1.00	580	164
700- 800	1.3×10^{-1}	4.9×10^{-3}	0.39	0.34	0.78	0.80	920	187
800- 900	1.3×10^{-4}	1.5×10^{-4}	0.52	0.62	1.04	0.72	2468	725
900-1000	6.1×10^{-6}	2.8×10^{-5}	0.47	0.48	0.94	0.56	2040	-48
1000-1100	1.6×10^{-5}	3.7×10^{-5}	0.51	0.52	1.02	0.74	1950	1546
			H_2O					
1100-1600	3.5×10	1.4×10	0.48	0.66	0.96	0.64	300	368
1600-2000	1.4×10	3.9×10	0.48	0.52	0.96	0.88	300	257

CONCLUDING REMARKS

The empirical transmitrance constants derived in this study should be useful for calculations of atmospheric radiation in planetary atmospheres containing carbon dioxide and water vapor. The path length and pressure dependencies of the transmittances are fit quite well by the modified strong line absorption law. However, the temperature dependence, represented by the coefficient γ, can be improved upon. Possible improvements in the fitting of the temperature dependence include the following methods, which are based upon determination of the temperature coefficients from the least squares fitting procedure. In the first method, the temperature dependence of the path would be assumed to be a factor of the form

$$\left(\frac{T_o}{T}\right)^{1.5} \exp\left[\gamma\left(\frac{1}{T_o} - \frac{1}{T}\right)\right] \quad .$$

In the second method, the temperature dependence would be assumed to be a simple power function of the form $(T_o/T)^{\ell}$. In either case, the empirical constants (γ in the first method, ℓ in the second method) would be calculated simultaneously with the other empirical constants, m, n, and k, from a least squares fitting procedure. This differs from the present study in which the temperature coefficient is calculated by an averaging method that is independent of the least squares procedure used to determine the other constants. It is expected that the spectral intervals with strong temperature dependence will follow the temperature dependence of method one, while the spectral intervals with weak temperature dependence will follow the simple power law. Such calculations are planned.

REFERENCES

1. Bartko, F., and R. Hanel, 1968: Non-gray equilibrium temperature distributions above the clouds of Venus. Astrophys. J., 151, 365-378.

2. Plass, G., and V. Stull, 1962: Carbon dioxide absorption for path lengths applicable to the atmosphere of Venus. Ford-Aeroneutronic Publ. No. U-1844.

3. Stull, V., P. Wyatt, and G. Plass, 1962: The infrared absorption of water vapor. AFSC Report. SSD-TDR-62-127, Vol. II.

4. Stull, V., P. Wyatt, and G. Plass, 1963: The infrared absorption of carbon dioxide. AFCS Report. SSD-TDR-62-127, Vol. III.

5. Ohring, G., 1969: Planetary Meteorology. Quart. Prog. Rept. No. 3, Contract NASW-1725, 76 pp.